




Channel-lobe transition zone development in tectonically active settings: Implications for hybrid bed development

Hannah L. Brooks^{1,2}  | Makoto Ito² | Valentin Zuchuat¹  | Jeff Peakall³ | David M. Hodgson³ 

¹EMR – Geological Institute, RWTH Aachen University, Aachen, Germany

²Department of Earth Sciences, Chiba University, Chiba, Japan

³School of Earth and Environment, University of Leeds, Leeds, UK

Correspondence

Hannah L. Brooks, EMR – Geological Institute, RWTH Aachen University, 52062 Aachen, Germany.

Email: hannah.brooks@emr.rwth-aachen.de

Funding information

Japan Society for the Promotion of Science London

Abstract

Channel-lobe transition zones are dynamic areas located between deepwater channels and lobes. Presented here is a rare example of an exhumed channel-lobe transition zone from an active-margin setting, in the Kazusa forearc Basin, Boso Peninsula, Japan. This Plio-Pleistocene outcrop exposes a thick (tens of metres) channel-lobe transition zone succession with excellent dating control, in contrast to existing poorly dated studies of thinner (metres) deposits in tectonically quiescent settings. This high-resolution outcrop permits the roles of climate and associated relative sea-level changes on stratigraphic architecture to be assessed. Three development stages are recognised with an overall coarsening-upward then fining-upwards trend. Each stage is interpreted to record one obliquity-driven glacioeustatic sea-level fall-then-rise cycle, based on comparison with published data. Deposition of the thickest and coarsest strata, Stage 2, is interpreted to record the end of a period of relative sea-level fall. The thinner and finer strata of Stages 1 and 3 formed during interglacial periods where the stronger Kuroshio Oceanic Current, coupled to increased monsoonally driven tropical cyclone frequency and intensity, likely resulted in inhibited downslope sediment transfer. A key aspect of channel-lobe transition zone deposits in this case is the presence of a diverse range of hybrid beds, in contrast to previous work where they have primarily been associated with lobe fringes. Here hybrid bed characteristics, and grain-size variations, are used to assess the relative importance of longitudinal and vertical segregation processes, and compared to existing models. Compared to channel-lobe transition zones in tectonically quiescent basin-fills, this channel-lobe transition zone shows less evidence of bypassing flows (i.e. thicker stratigraphy, more isolated scour-fills, fewer bypass lags) and has significantly more hybrid beds. These features may be common in active basin channel-lobe transition zones due to: high subsidence rates; high sedimentation rates; and disequilibrium of tectonically active slopes. This disequilibrium could rejuvenate erodible mud-rich substrate, leading to mud-rich flows arriving at the channel-lobe transition zone, and decelerating rapidly, forming hybrid beds.

This is an open access article under the terms of the [Creative Commons Attribution](https://creativecommons.org/licenses/by/4.0/) License, which permits use, distribution and reproduction in any medium, provided the original work is properly cited.

© 2022 The Authors. *The Depositional Record* published by John Wiley & Sons Ltd on behalf of International Association of Sedimentologists.

KEYWORDS

channel-lobe transition zone (CLTZ), glacioeustasy, hybrid beds, Kazusa Group, Pleistocene

1 | INTRODUCTION

Deepwater siliciclastic depositional systems can be simply divided into (i) a slope dominated by erosion and bypass processes (Galloway, 1998; McHargue et al., 2011; Prather, 2003; Stevenson et al., 2013) and (ii) a basin-floor dominated by depositional processes (Posamentier, 2003; Prélat et al., 2009; Sixsmith et al., 2004). At the critical zone of transition between these two areas, which typically coincides with the base-of-slope, deposits can either show characteristics typical of both the slope and basin-floor (Brooks et al., 2018a; Gardner et al., 2003; Van der Merwe et al., 2014), or are identified by their own separate recognition criteria (Brooks et al., 2018a, 2018b; Hofstra et al., 2015; Ito, 2008; Pemberton et al., 2016; Wynn & Stow, 2002; Wynn et al., 2002). This area is referred to as the channel-lobe transition zone (CLTZ; Mutti & Normark, 1987, 1991; Wynn et al., 2002), which has been defined as 'the region that, within any turbidite system, separates well-defined channels or channel-fill, from well-defined lobes or lobe facies' (Mutti & Normark, 1987). While CLTZs at breaks of slope are focussed on from hereon, they can also occur on the basin-floor well beyond the slope break (Droz et al., 2020).

Channel-lobe transition zones have been reported in detail from modern seafloor systems (Droz et al., 2020; Kenyon & Millington, 1995; Maier et al., 2018, 2020; Morris et al., 1998; Normark et al., 1979; Palanques et al., 1995; Wynn & Stow, 2002; Wynn et al., 2002), and from both tectonically quiescent and tectonically active settings, but it remains unclear how the CLTZ is affected by ongoing tectonic activity. Maier et al. (2018), for example, showed that, in a tectonically active and confined basin offshore southern California (USA) the CLTZ is influenced by antecedent basement topography and active fault systems. This resulted in: limited avulsion, as the channel is locked between basement highs; formation of a scour field; narrow disconnected channels with knickpoints; and sediment waves plus stacked lobes formed in areas of lower gradient in the basin as well as along the basin margins (Maier et al., 2018). Therefore, CLTZ dynamics are clearly significantly affected by the basinal setting in which they form and syn-sedimentary tectonism.

Ancient examples of CLTZs are challenging to identify and require a well-constrained palaeogeographic context (Mutti & Normark, 1987). Nevertheless, outcrop studies (Brooks et al., 2018a, 2018b; Hofstra et al., 2015; Ito, 2008; Pemberton et al., 2016; Pyles et al., 2014; Van der Merwe

et al., 2014) have helped develop recognition criteria for CLTZs, which include: a thin stratigraphic expression; amalgamated erosional features; coarse-grained/mudclast lag deposits; aggradational bedforms (i.e. sediment waves); soft-sediment deformation; interfingering of up-dip and down-dip deposits; and sand-rich hybrid beds in proximal lobes (Brooks et al., 2018a; Mansor & Amir Hassan, 2021; Stevenson et al., 2015). Detailed outcrop research on CLTZs has often focussed on large, relatively tectonically quiescent basins associated with mature passive margins, or thermal sag basins, such as the Karoo Basin in South Africa (Brooks et al., 2018a; Hofstra et al., 2015; Van der Merwe et al., 2014). Therefore, it is important to understand if these same models can be applied to tectonically active basins, such as forearc, or retroarc foreland basins, as well as understanding the influence of tectonism under different depositional climates.

Regional work by Ito (2008) on a 20 km dip transect of an exhumed CLTZ in the Plio-Pleistocene Otadai Formation, deposited in the active Kazusa forearc Basin, Japan, also suggests that the sedimentology and architecture of a CLTZ differs in an active forearc basin setting compared to tectonically quiescent basins. Specifically, Ito (2008) focussed on the downflow transition of beds from turbidites to hybrid beds, and back to turbidites downslope through this system. Ito (2008) documented numerous hybrid beds within the stratigraphy downflow of the channel mouth, the prevalence and variability of which contrast with hybrid beds observed in the Karoo Basin (Brooks et al., 2018a). Furthermore, the thickness of deposits (*ca* 100 m) indicates a strongly aggradational setting (Ito, 2008). Typically, these young sediments (1.18–0.9 Ma) are poorly cemented and have undergone minor diagenesis (Kajita et al., 2021), and therefore are well-suited to detailed grain-size analysis.

Currently, there is limited grain-size data available for deep-marine outcrops (Stevenson et al., 2014a), with the majority collected from thin-section analyses (Lowe & Guy, 2000; Stevenson et al., 2020; Sylvester & Lowe, 2004). The presence of authigenic clay minerals coupled with cementation and metamorphism in many other studies complicate the recognition of detrital clays present within the flow. Nevertheless, studies on turbidites and associated debrites have shown that the analysis of mud in thin sections supports the observations of mud in the field (Bell et al., 2018; Kane et al., 2017; Lowe & Guy, 2000; see Stevenson et al., 2020 for full discussion). The present study is not restricted by these limitations, and is used to

provide an extensive analysis of the grain-size distributions and their formative processes.

This study examines a thick stratigraphic section (100 m) in order to establish a sedimentological and stratigraphic architectural model for CLTZs in forearc basins. The objectives of this study are: (i) to document the bed types, architecture and evolution of an exposed CLTZ from a tectonically active system; (ii) to record and discuss the extent of recorded bed types, and the distribution of hybrid beds within this zone; (iii) to identify and discuss the factors controlling the formation and evolution of this zone (e.g. seismicity, glacioeustasy and climate change) using comparisons to other systems globally; and (iv) to summarise these into conceptual models of CLTZ architecture in tectonically active and quiescent margins.

2 | GEOLOGICAL SETTING

The Kazusa Basin developed as a forearc basin in response to the subduction of the Pacific and Philippine Sea plates beneath the Eurasia plate, which resulted in the formation of the Izu-Bonin Trench and Sagami Trough (Ito & Masuda, 1989; Katsura, 1984) during the latest Pliocene to Quaternary (Takano et al., 2004). The basin was filled with the 3 km thick primarily siliciclastic marine succession of the Kazusa Group (Figures 1 and 2; Takano et al., 2004). The Kazusa Group strata display an overall shallowing-upward trend from deep-marine to shallow-marine environments, reflecting an overall transgressive to regressive cycle. The whole group consists of 17 high-frequency depositional sequences/cycles (comprising the stratigraphy shown in Figure 1B), interpreted to be formed by the interaction of glacioeustatic sea-level changes and forearc tectonics (Ito, 1996; Ito & Katsura, 1992; Katsura, 1984). Overall, this basin is characterised by a fast rate of sediment accumulation (an average for the entire Kazusa Group of up to 4.9 m/kyr; Pickering et al., 1999). The subsidence rate during the formation of the basin (2.4–0.45 Ma) is estimated to have peaked at <2.5 m/kyr (Kaizuka, 1987; Naruse, 1968). The Kazusa Group has been separated into 23 different lithostratigraphic formations (Horikawa & Ito, 2004), notably including the Otadai Formation (Figure 1B), which is the main focus of this study. These deposits have been uplifted to form outcrops onshore at the present day, with some upper Pleistocene coastal deposits (*ca* 0.12 Ma) being uplifted up to 100 m above present-day sea level, with an average uplift rate of *ca* 0.8 m/kyr (Kaizuka, 1987).

The Otadai Formation reaches a maximum thickness of 520 m and is estimated to have been deposited

between 1.18 and 0.9 Ma (Figure 1B) based on biostratigraphy, magnetostratigraphy and fission-track dating of volcanic ash beds (Takano et al., 2004). The Otadai Formation is dominated by gravity flow deposits, which formed a submarine fan system (Hirayama & Nakajima, 1977; Katsura, 1984), fed by a channel/canyon system that crops out to the south-west of the study area in the up-dip section of the Otadai and Higashihigasa formations (Figure 2A,B; Ito & Saito, 2006; Ito et al., 2014). The Otadai Formation has been subdivided into four 110–130 m thick sequences, each containing a lower sandstone-dominated interval and an overlying siltstone-dominated interval, which are interpreted to represent periods of low and high sea level respectively (Figure 2B; Ito, 1998a, 1998b; Ito & Katsura, 1992). This relationship is likely complicated by regional climate factors, such as variations in monsoonal activity (Nakajima et al., 2009), and tropical cyclone frequency and intensity. Correlation between outcrop sections is possible through the regional identification and dating of volcanic ash marker beds (Figure 2B; Ishiwada et al., 1971; Machida et al., 1980; Mitsunashi, 1954, 1961; Mitsunashi et al., 1959; Satoguchi, 1995; Satoguchi & Nagahashi, 2012).

3 | STUDY LOCATION

This study focusses on the top of Sequence 6 and Sequence 7 (Figure 2C) of the Kazusa Group (the third sequence of the Otadai Formation), deposited during Marine Isotopic Stage MIS-32 (Kajita et al., 2021; Saganuma et al., 2021) to MIS-30 (Pickering et al., 1999), in a location interpreted as a CLTZ (Figure 2A; Location 2 of Ito, 2008). This cycle consists of a 90 m thick siltstone to sandstone-dominated interval, interpreted as the falling stage and lowstand systems tract. This is followed by a 50 m thick, siltstone-dominated interval interpreted as the transgressive and highstand systems tracts (Figure 2C; Ito, 2008). The sandstone-dominated interval comprises medium (0.1–0.3 m), thick (>0.3–1 m) and very thick (>1 m) beds, with a high proportion of intraformational clasts (pebble to boulder grade), as well as minor, thin (<20 cm thick) siltstone beds and pumice/ash layers, sourced from volcanoes that were active in the vicinity of the depocentre at the time (Kikkawa et al., 1991; Machida et al., 1980) (Figure 2C). The regionally correlated ash bed O16 (1.10 Ma; Suzuki & Sugihara, 1983) and ash bed O11 (1.07 Ma; Suzuki & Sugihara, 1983) are present near the base and near the top of the measured section in Location 2 respectively (Figure 2B,C). The siltstone-dominated interval comprises thin-bedded (centimetres) to medium-bedded (decimetres) siltstone,

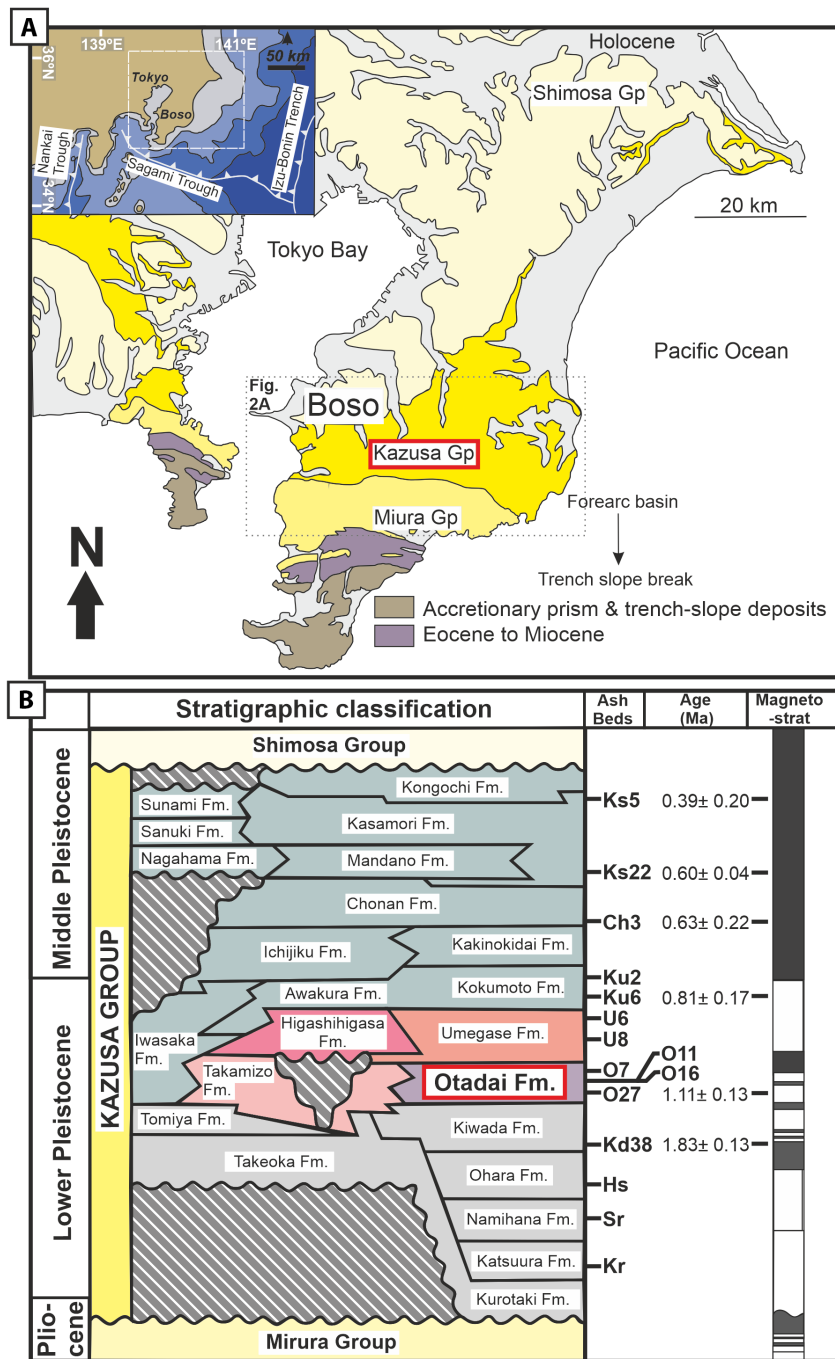


FIGURE 1 (A) Geological map of the Boso Peninsula, Japan and adjacent areas (Modified from Ito et al., 2016). Inset map shows a modern plate tectonic framework of the Boso Peninsula. (B) Stratigraphic column of Kazusa Group (Modified from Ito, 2008), see Horikawa and Ito (2004) for data sources. Red box highlights the studied formation

with some intercalated thin-bedded to medium-bedded, finer-grained sandstones (Figure 2C). The measured section is estimated to span 30 kyr (Suzuki & Sugihara, 1983), while the whole of Sequence 7 (sandstone and mudstone-dominated interval) is estimated to represent 50 kyr years of deposition (Ito, 1998a, 2008; Ito & Katsura, 1992; Takano et al., 2004). The main focus of this study is on the area recognised as the CLTZ (Figures 2A and 3A,C; Location 2 of Ito, 2008), with a section that is located 4 km up-dip, interpreted as channel overbank deposits (Figure 2A,B; Location 1 of Ito, 2008), used for comparison.

4 | METHODOLOGY

The section at Location 2 (as named in Ito, 2008) was logged in detail along a river cut (Figure 3A,C) from the base of Sequence 7 from the regionally extensive O16 ash bed, up to the O11 ash bed present within the overlying siltstone-dominated section (Figure 2C). A less detailed stratigraphic log was documented from a river cut 4.5 km up section (Figure 3A,B; Location 1 in Ito, 2008) to compare changes within packages; no samples were taken at this location. Logged sections record information on the lithology, grain size, sedimentary

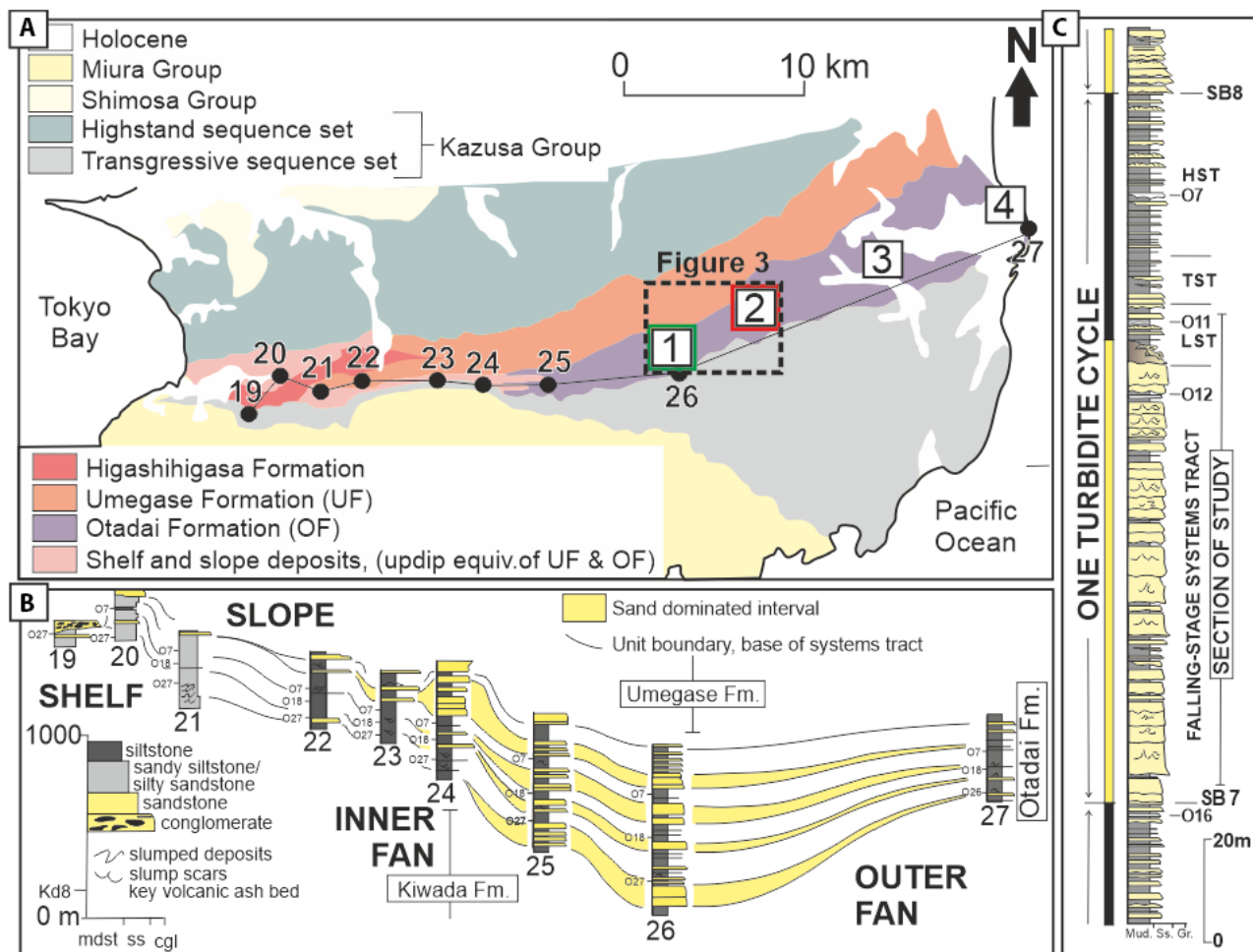


FIGURE 2 (A) Geological sketch map of central Boso Peninsula. Modified from Ito (1998a) and Ito (2008). Location numbers 1–4 indicate areas proximal to distal studied by Ito (2008), this study focusses on locations 1 and 2, see Figure 3 for satellite imagery of location. (B) Stratigraphic cross-section and sequencestratigraphic framework of the Kazusa Group demonstrating shelf to outer fan correlation, position of logs shown in (A), modified from Takano et al. (2004). O7 to O27 are regionally extensive ash beds used for correlation. (C) Sketch log and sequence stratigraphic characterisation of a ‘mid-fan’/base-of-slope section of the Otadai Formation. O7 tephra estimated at 1.05 Ma; LST—Lowstand systems tract, TST—Transgressive systems tract, HST—Highstand systems tract, SB7—Sequence boundary 7, SB8—Sequence boundary 8 (modified from Tsuji et al., 2005), key shown in (B)

structures, bed architecture and stratal boundaries at centimetre-scale resolution. Standard techniques in lithofacies and architectural-element analysis (*sensu* Walker, 1992) were used to identify and interpret the different processes involved in the deposition of the targeted interval (Tables 1 and 2). Grain-size samples were used to assess variations in grain size and mud content across the whole section, as well as between different bed types. Within each sampled bed, samples were collected at roughly 20 cm intervals from the bed base; 61 samples from 12 beds were analysed in total. The Otadai Formation consists of young, shallow buried, un lithified sediments, which has prevented them being affected by intense deformation and only minor diagenetic alteration is present (Inami, 1981; Kajita et al., 2021; Kase et al., 2016), including limited amounts of

carbonate cement. An estimated 45°C maximum palaeotemperature and 960 m maximum burial depth (similar to the present-day overburden; Kamiya et al., 2017) support this. Therefore, sediment samples from the studied sections were easily disaggregated and deflocculated with addition of sodium hexametaphosphate (0.05% solution) under ultrasonic vibration in a water bath (for 2 min). The sample mixture was transferred to the Mastersizer 3000 grain-size analyser where the integrated stirrer and ultrasonic vibration ensured an evenly mixed suspension of grains. The grain size of the collected material was measured using laser diffraction grain-size analysis. The Mastersizer 3000 measures particles in the range of 10 nm to 3500 µm, coarser samples were passed through a 3500 µm sieve before measuring, these grains were found to be aggregate grains and

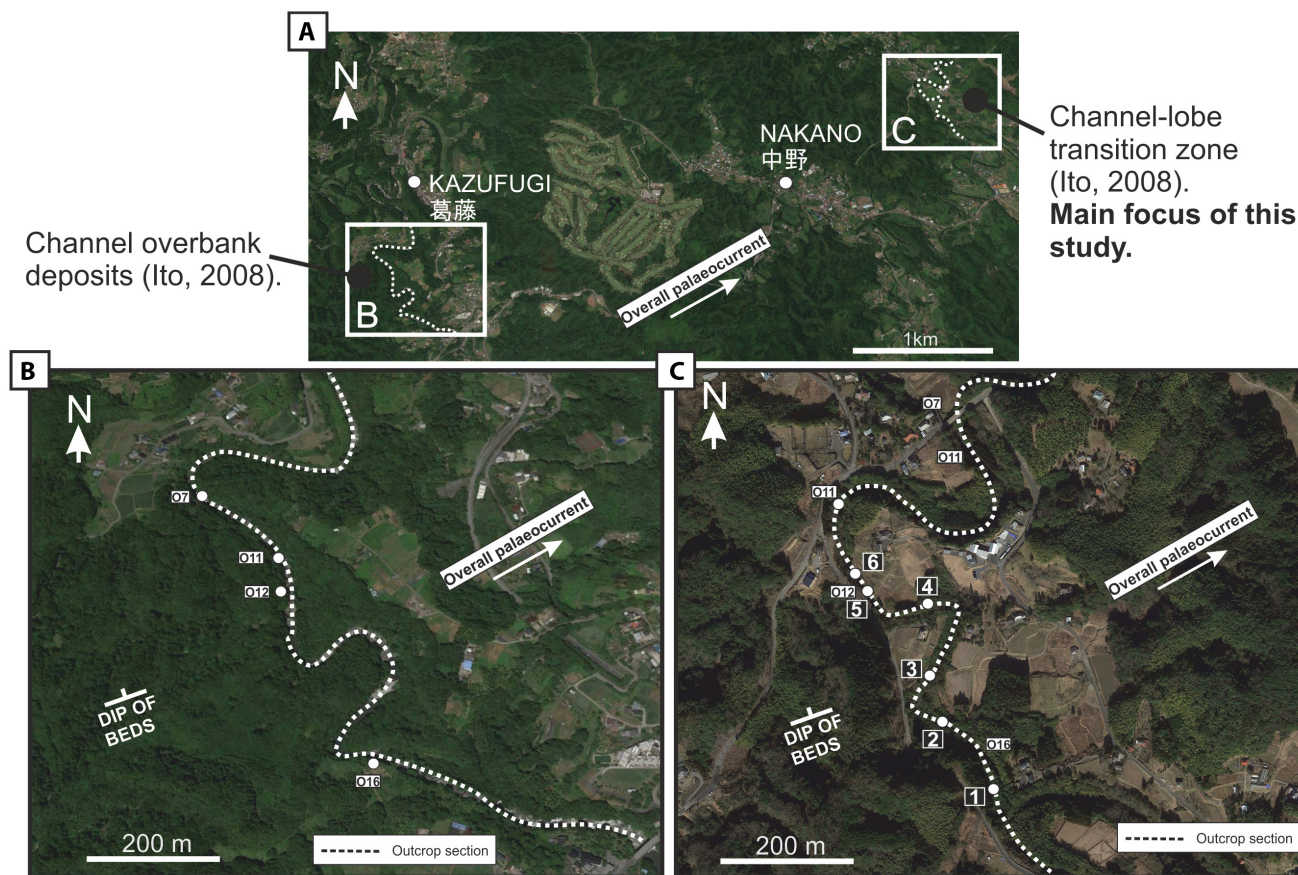


FIGURE 3 (A) Google Earth image showing location in dashed black box (Figure 2A) of location 1 (B) and location 2 (C) as named by Ito (2008). These are interpreted as channel overbank deposits and channel lobe transition zone deposits respectively. This study examines the channel-lobe transition zone deposits of location 2 in more detail with location 1 used for comparison. (B) Google Earth image of logged river section (Location 1, Ito, 2008) O7, O11, O12 and O16 are regionally extensive ash beds used for correlation. (C) Google Earth image of logged river section (Location 2, Ito, 2008) O7, O11, O12 and O16 are regionally extensive ash beds used for correlation; numbers denote sections shown in Figure 6

negligible. Using the Mastersizer 3000, each sample was circulated five times through the grain-size analyser, and an average of these five measurements was used as the final result.

4.1 | Sampling and detailed grain-size analysis

Tables 3 and 4 display the detailed results of the grain-size analysis for the samples of bed types 1 through 3 in order to support the subdivision of these groups. Table 3 displays a sketch log of each bed sampled, and the location of each sub-sample. Table 4 shows the corresponding numerical data. For each sample, the d_{50} (particle diameter representing the 50% cumulative-percentile value) and average standard deviation (ASD) were measured. The ASD is a measure of the data spread in micrometres (μm), which can be used as a proxy for sorting (Friedman, 1962). The relative standard deviation (RSD)

is a comparison of the ASD with the average grain size (d_{50}), expressed as a percentage, enabling a better assessment of sorting between samples. To obtain the RSD, the standard deviation is multiplied by 100, and this product is divided by the average.

The mud content is defined as the combined clay and silt content (grain sizes of $<63 \mu\text{m}$; McCave et al., 1995; Winterwerp & van Kesteren, 2004). The clay content (grain sizes of $<4 \mu\text{m}$) was also measured through each bed to aid interpretation of flow variation during bed deposition. The overall grain-size distribution for each sub-sample is displayed on a logarithmic volume-density-distribution graph (Table 3). Single peaks indicate a unimodal sorting, with a narrow grain-size range; convex shapes indicate a broader grain-size spread; and flatter curves reflect a more equal proportion of different grain sizes. The detailed grain-size information, descriptions and interpretations of each sample are given in Table 2 and Material S1, these are integrated into bed type interpretations below.

TABLE 1 Facies codes, names, descriptions and interpretations. See Material S1 and Table 2 for bed types and corresponding facies

Facies code	Facies	Description	Interpretation
LM	Laminated mudstone	Dark brown to grey, clay to silt-grade, crudely to well-laminated. Sporadic mm sized pumice and shell fragments can be present. See example at top of Figure 4Ai	Deposition from suspension fall-out. Background sedimentation or settling from tail of turbidity current
DM	Debritic mudstone	Clay and siltstone matrix with clasts mm- 10 cm consisting of sandstone, mudstone, pumice and organic material. Often dewatered/ loaded contact with sandstone facies below. See example in Figure 4Di	<i>En masse</i> deposition from a cohesive flow (Haughton et al., 2009)
SS	Structureless sandstone	Fine- coarse sandstone, well to- moderately well-sorted. Loaded or erosional bases common. Can fine upwards. See example in Figure 4Civ	Rapid suspension fall-out from high-density turbidity current (Lowe, 1982)
PLS	Parallel laminated sandstone	Medium- to very finer-grained sandstone, with horizontal laminations picked out by subtle changes in colour or grain size	Tractional laminations formed by a waning flow (Allen, 1983)
RS	Rippled sandstone	Medium- to very finer-grained sandstone with asymmetrical ripple laminations, 1–5 cm thick and 5–10 cm in wavelength. See example in Figure 4Cii	Current ripples through tractional reworking in a decelerating turbulent flow
BSMP	Banded sandstone, mudstone and pumice	Bands 1–10 cm thick, consisting of coarse, medium and fine sandstone, siltstone, clay as well as organic-rich layers and granule sized pumice. See examples in Figure 4Ai and Aii	Deposition from mud-rich transitional flow (see text for full interpretation)
SCL	Sandstone with convoluted laminations	Fine to very finer-grained sandstone with parallel, wavy and convoluted laminations. Often occurs overlying a sharp grain-size break, and fines up into laminated mudstone facies. See example in Figure 4Bvi	Shear, buoyancy instabilities, and/or water escape (Gladstone et al., 2018 and references therein)
SML	Sandstone with mudclast layers	Coarse- to finer-grained sandstone, well- to poorly sorted containing randomly orientated to imbricated mudclasts. Clasts are mm to boulder in size. Layers of clasts can be cm's to dm's thick. Layers can be singular or multiple. See example in Figure 4Ciii	High-density turbidity currents with mudclasts transported as bedload
DSM	Deformed sandstone and mudstone	Deformed structured coarse to very finer-grained sandstone, siltstone and claystone. Structures include parallel and ripple laminations that are contorted. Can include dish structures, loading and pipes. See example in Figure 4Biii	Slumping and remobilisation of soft sediments, along with dewatering
MCC	Mudstone clast conglomerate	Up to 80% by volume mudclasts, gravel to boulder in size. Sub-angular to sub-rounded, randomly orientated. See example in Figure 4Bii.	Ripped up beds (Cunha et al., 2017) or rafts (Fonnesu et al., 2018)
A/T	Ash/tephra	White or black very finer-grained ash, within thin mm to cm laminations, marked by small changes in colour. Pumice, silt grains and sand grains are intercalated within the bed in undulating layers 1–5 cm in thickness. Ripple laminations can be present. See example in Figure 4E	Settling from suspension of ash fall from local volcanic eruptions. Intercalated sediments from low-density turbidity currents and hemipelagic sediment

5 | BED TYPES

This section presents a detailed description and interpretation of the different bed types recognised in this study (Material S1, Table 2, Figure 4) in order of occurrence, from base to top of the measured section. Information on individual facies can be found in Table 1, with examples in Figure 4. Five 'Bed Types' (BTs 1–5) represent groups of beds that have similar characteristics for purposes of interpretation. Note that BT 2 was separated into three

groups (BTs 2i, 2ii and 2iii) based on thickness, evidence of remobilisation (e.g. soft-sediment deformation) and occurrence of bioturbation.

5.1 | BT 1—Banded beds (Sample 6)

Description: Bed type 1 (sub-types A, B; Material S1, Table 2; Figure 4Ai,ii) are thin to medium thickness (<40 cm) and consist primarily of sandstone. Within these sandstones,

TABLE 2 Abbreviated table listing bed types and subdivisions, including a description, bed thickness and sedimentary structures. Full table can be seen in Material S1, with additional representative sketches of each bed type. Information of facies can be found in Table 1. Information on samples can be found in Tables 3 and 4

Bed types (Facies code, Table 1)	Description	Bed thickness	Structures (see caption for codes)
1. Banded beds (LM, BSMP, SS, PLS, SCL)	A (Figure 4Ai) (S3, S6)	Banded sandstone/siltstone beds. Bands 1–10 cm thick. Sharp (bed) top and base contacts. Clay to granule size particles. Alternating between lighter ‘sandy’ bands (with silt-/sandstone, pumice and mudclasts) and darker ‘muddy’ bands (mostly clay-/siltstone)	4–40 cm Ba., R.L., Lo.
	B (Figure 4Aii)	Banded granule, sandstone and siltstone beds. Sharp bed tops and erosive bed bases. Base of poorly sorted medium to coarse sandstone. Overlain by fine to medium sandstone with mudclasts and pumice. 5–40 cm banded intervals occur near top of bed. Bands as 1A. Bands are sometimes discontinuous and forming undulating ‘wave’ like features	30–50 cm Ba., undulating gravel ‘waves’, Lo., R.L.
2i. Hybrid beds (LM, SS, PLS, RS, BSMP, SCL, SML, DSM, MCC)	C (S1, S5, S10)	Bipartite beds. Sharp, erosional base and top. Beds pinch out laterally. Commonly sole structures on base of beds. Lower Division: poorly sorted fine to coarse sandstone structureless or structured. Upper division: poorly sorted silt to very fine sandstone with mm- cm clasts	8–50 cm Sc., Fl., Gr., D.S., R.L., P.L.
	D (S4)	Bipartite beds. Sharp, erosional base and top. Commonly sole structures on base of beds. Lower Division: thick poorly sorted medium to coarse sandstone. Overlain by grain-break to very fine sandstone with undulating clast layer. Upper division: same as C	ca 1 m Sc., Fl., Gr., Clast layer (gran-peb).
	E (S7, S11)	Bi/tripartite beds. Sharp, erosional base and top. Lower Division (not always present): gravel to boulder clasts, up to 80% clasts by volume. Middle division: poorly sorted fine to coarse sandstone with occasional gravel. Beds structureless or structured. Fines upwards to fine/very fine sandstone with some pumice. Upper division: same as C	0.3–2 m Sc., Fl., Gr., Clast layers (grav.-boul.), D.S., Lo.
	F (S13)	Bi/tripartite beds. Sharp, erosional base and top. Lower Division: same as E. Middle division: poor to moderately sorted medium sandstone to gravel. Beds structureless or structured. Can contain gravel- to boulder-sized mudclast layers. Can fine upwards to very fine sandstone with banded layers of siltstone and pumice with dewatering structures. Upper division: same as C	0.3–1.2 m Sc., Fl., Gr., Clast layers (grav.-bould.), D.S, C.L.
2ii. Megabeds (DM, LM, SS, PLS, RS, BSMP, SCL, SML, DSM, MCC)	G (S8)	7 distinctive thick beds. Siltstone to boulder-sized clasts. Beds vary in grain size and thickness laterally. Beds consist of amalgamated beds from other bed types and mudclast layers. See full table (Material S1) for full information	2.4–4.1 m Various (as above), Folds, Am.
2iii. Bioturbated hybrid beds (DM, SS, PLS, RS, BSMP, SCL, SML)	H (S14)	Bipartite beds. Sharp base and top. Lower Division: very-fine to medium sandstone, fining upwards. Banded intervals of very fine and fine sandstone, throughout or at top of beds. Can contain gravel to pebble-sized mudclast layers. Mm-sized organic matter fragments present dispersed throughout the beds. <i>Planolites</i> and <i>Thalassinoides</i> burrows common, burrowing index 2–3 (MacEachern et al., 2005). Upper division: same as C	0.3–1 m Lo., R.L, C.R.L.,

TABLE 2 (Continued)

Bed types (Facies code, Table 1)	Description	Bed thickness	Structures (see caption for codes)	
3. Low-density turbidites to high-density turbidites (LM, SS, PLS, RS, BSMP, SCL, SML)	I (S2)	Very fine to coarse sandstone beds with sharp, erosional base and top. Poorly sorted base. Beds fine upwards. Scours can be gravel-infilled. Overlying this, beds contain medium to very coarse, poorly sorted sandstone, with mudstone and debrite clasts (pebble to boulder). Clast layers can form discontinuous undulating 'wave' like features. Top often fines upwards to structured fine to very-fine sandstone	0.3–1.2 m	Sc. Fl., Gr. Am., undulating gravel 'waves', C.L., L.S., C.R.L.
	J (S12)	Coarse to very fine sandstone beds. Bases consist of poorly sorted medium to coarse sandstone. Beds fine upwards to very fine sandstone with structures	0.2–1.5 m	Sc. Fl., Gr., Am., C.R., C.L.
	K (S9)	Very fine sandstone beds, occasionally with gravel. Base consists of poorly sorted medium to coarse sandstone with shell fragments. Beds fine up to structured very fine sandstone, with intervening discontinuous clast layers (coarse sandstone, gravel and pumice) marking a sharp grain-size break. Beds are capped by a siltstone layer which loads into the sandstone below.	1–1.2 m	Sc. Fl., Gr., Clast layers, C.L., Lo.
	L	Poorly sorted siltstone to pebble beds. Erosional and undulating base, sharp and undulating top. Coarse sandstone and gravel at bed bases. Beds fine upwards to medium/fine sandstone with mudclast pebbles and structures, and then structureless very fine sand/siltstone	ca 1 m	Sc., C.L., L.S.
4. Debrites (DM, DSM, MCC)	M	Very poorly sorted beds, siltstone to boulder-sized clasts. Erosive scoured base, undulating top. Lateral bed thickness changes. Matrix: siltstone to gravel, shell fragments and pumice. Clasts: Gravel to boulder-sized mudstone clasts, 50%–70% by volume, angular to sub-rounded, randomly orientated. <i>Planolites</i> , <i>Thalassinoides</i> and <i>Chondrites</i> are present, burrowing index 3–4 (MacEachern et al., 2005)	1–1.5 m	Folds
5. Ash/Tephra (A/T)	N	Ash beds. Sharp planar non-erosive base and top. Very fine grained, black or grey-white in colour. Minor siltstone, organic matter, pumice and scoria. Can contain dark grey/black ash layers mixed with siltstone. <i>Planolites</i> , <i>Thalassinoides</i> and <i>Chondrites</i> are common, burrowing index 2–4 (MacEachern et al., 2005)	10–40 cm	R.L. (low angle)

Code for structures: Ba. = Banding, R.L. = Ripple lamination, Lo. = Loading, Sc. = Scours, Fl. = Flutes, Gr. = Grooves, D.S. = Dish structures, P.L. = Planar laminations, C.L. = Convolute laminations, C.R.L. = Climbing ripple laminations, L.S. = Loading structures, A.M. = Amalgamation surfaces.

there are alternations of siltstone-rich and claystone-rich darker bands and sandstone-rich and pumice-rich lighter bands; these occur throughout or near the tops of beds. Minor dewatering structures and ripple laminations are present at the tops of beds. For a full description see Tables 1 and 2.

Interpretation: The mechanisms for forming 'bands' have been debated. Lowe and Guy (2000) proposed that banding develops at the base of flows that vary between turbulent and laminar states, through the cyclic development of near-bed cohesive plugs. In contrast to this, experimental work on transitional flows (*sensu* Baas et al.,

2009) with well-developed cohesive plugs has demonstrated that banded deposits can form within the upper stage plane bed flow regime, and at the transitional zone between true ripples and upper stage plane beds (Baas et al., 2011, 2016; Baker & Baas, 2020). Transitional plug flows progressively form as increasing amounts of cohesive clay within the flow modifies turbulence (from enhanced to damped). This results in the development of a laminar plug, which grows downward from an interval of low shear stress (Baas et al., 2009). This transitional-flow behaviour is governed by the balance of turbulent

TABLE 3 Sample numbers and corresponding bed type code, grain-size mean and standard deviation for each sample, sketch log showing location of each sample within the bed, % volume silt and clay content of the bed and grain-size distribution curves for each sample

Bed Type	Samp. no.	Mean & Standard Deviation	Sketch log	Silt (<63 μm) & clay (<4 μm) content	Grain size distribution
A	S3	<p>3.2 3.1</p>		<p>3.2 3.1</p>	<p>CLAY SILT SAND</p>
A	S6	<p>6.2 6.1</p>		<p>6.2 6.1</p>	
C	S1	<p>1.3 1.2 1.1</p>		<p>1.3 1.2 1.1</p>	
C	S5	<p>5.2 5.1</p>		<p>5.2 5.1</p>	
C	S10	<p>10.2 10.1</p>		<p>10.2 10.1</p>	
D	S4	<p>4.5 4.4 4.3 4.2 4.1</p>		<p>4.5 4.4 4.3 4.2 4.1</p>	
E	S7	<p>7.10 7.9 7.8 7.7 7.6 7.5 7.4 7.3 7.2 7.1</p>		<p>7.10 7.9 7.8 7.7 7.6 7.5 7.4 7.3 7.2 7.1</p>	

TABLE 3 (Continued)

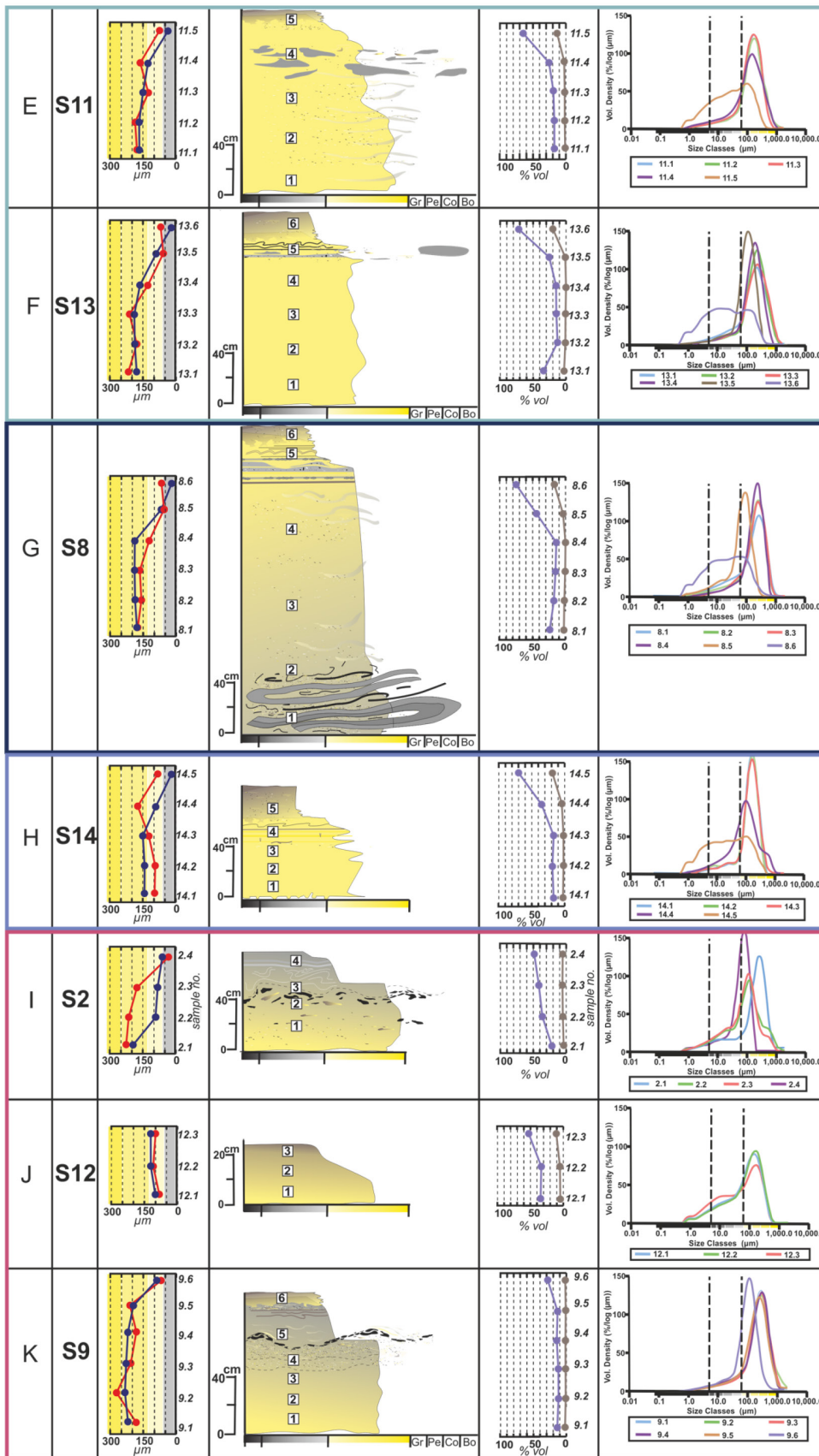


TABLE 4 Laser diffraction grain-size analysis results for samples. Showing bed types, sample numbers, sub-sample (within bed), d(50), average standard deviation (ASD), relative standard deviation (RSD), the results below 63 μm (silt and clay), results below 4 μm (clay), d(90) and d(10). Notes show any other useful information, see text for details. Graphs of results and sketch of bed with location of sub-samples shown in Table 3. Detailed description of each bed type can be found in Material S1 and an abridged version in Table 2

Bed types	Sample no.	Sub-sample	d(50) (μm)	ASD (μm)	RSD (%)	Result Below (63) μm (%)	Result Below (4) μm (%)	d(90) (μm)	d(10) (μm)	Notes		
A	3	3.2	64.4	70.8	110	48.87	2.52	167	15.6	Sand-rich band		
		3.1	64.5	51	79	48.61	4.02	136	12.1			
A	6	6.2	19.3	25.9	134	89.95	16.23	63.1	2.52	Mud-rich band		
		6.1	70.6	89.6	127	43.68	3.54	160	14.2			
C	1	1.3	33	96.4	292	65.33	12.79	197	3.14	H3b?		
		1.2	50.6	114	225	57.32	6.18	244	6.78	H3a?		
		1.1	74.6	84.1	113	42.43	2.86	205	15.6	H1		
C	5	5.2	32.8	79.8	243	66	12.37	176	3.25	H3		
		5.1	65	59.1	91	48.47	4.65	154	9.96	H1		
C	10	10.2	36.9	94.9	257	62.39	11.35	209	3.52	H3		
		10.1	209	254	122	19.22	1.54	565	25.2	H1		
D	4	4.5	14.5	29.3	202	89.5	20.01	64.6	2.1	H3		
		4.4	262	241	92	16.6	1.99	611	28.7	H1		
		4.3	194	201	104	28.57	4.4	499	9.64	H1- Clast Layer		
		4.2	258	303	117	20.01	2.92	673	17.1	H1		
		4.1	235	292	124	23.69	3.66	650	12.5	H1		
E	7	7.10	29.6	56.7	192	69.12	14.39	137	2.8	H3b?		
		7.9	44.1	70.8	161	59.98	8.71	176	4.59	H3a?		
		7.8	140	223	159	21.49	2.23	528	22.1	H1- Clast Layer		
		7.7	177	176	99	16.65	2.09	435	28.2	H1		
		7.6	203	151	74	15.31	1.35	426	32.8	H1		
		7.5	212	160	75	14.61	1.8	445	33.3	H1		
		7.4	212	150	71	13.45	2.22	436	38.8	H1		
		7.3	201	159	79	15.94	2.76	421	26.1	H1		
		7.2	208	145	70	14.29	1.48	422	35.6	H1		
E	11	7.1	201	132	66	12.61	0.99	396	46.6	H1		
		11.5	30.9	74.2	240	65.76	13.55	169	3	H3		
		11.4	132	165	125	25.56	2.99	404	16.2	H1- Clast Layer		
		11.3	150	134	89	18.67	1.69	350	28.6	H1		
		11.2	164	192	117	16.5	1.44	425	33.1	H1		
		11.1	163	175	107	17.29	1.3	401	31	H1		
		F	13	13.6	18.9	70.8	375	72.86	19.23	152	2.19	H3
				13.5	94.1	56	60	25.84	1.69	176	29.2	H2
				13.4	162	126	78	15.46	0.91	354	36.2	H1
13.3	197			208	106	15.03	1.1	537	35.6	H1		
13.2	194			180	93	12.75	1.25	468	46.7	H1		
13.1	171			212	124	20.79	2	502	20.9	H1		

TABLE 4 (Continued)

Bed types	Sample no.	Sub-sample	d(50) (µm)	ASD (µm)	RSD (%)	Result	Result	d(90) (µm)	d(10) (µm)	Notes
						Below (63) µm (%)	Below (4) µm (%)			
G	8	8.6	20.2	67.2	333	75.52	17.5	123	2.36	H3
		8.5	69.9	52.1	75	44.45	4.65	146	9.5	H2
		8.4	192	126	66	14.1	1.05	379	39.2	H1
		8.3	200	161	81	15.64	0.97	446	37.8	H1
		8.2	191	158	83	18.47	2.38	426	22.6	H1- Clast Layer
		8.1	177	172	97	24.97	2.7	447	15	H1- Clast Layer
H	14	14.5	23.3	83	356	69.32	18.05	172	2.29	H3
		14.4	93.7	175	187	34.99	3.77	372	12	H2
		14.3	153	123	80	16.06	1.99	315	27.2	H1
		14.2	146	99.9	68	18.38	1.99	283	20.6	H1
		14.1	148	96	65	16.52	1.63	286	26.6	H1
I	2	2.4	64.4	39.7	62	48.58	4.17	122	12.1	
		2.3	80.8	137	170	41	5.11	261	8	Clast layer
		2.2	95.5	212	222	36.18	4.47	409	9.22	Clast layer
		2.1	196	227	116	21.73	3.39	447	12.3	Clast layer
J	12	12.3	33.5	97.4	291	61.18	13.52	220	2.99	
		12.2	112	133	119	33.55	4.54	326	9.49	
		12.1	110	120	109	33.73	4.34	307	9.83	
K	9	9.6	96.4	78.1	81	27.07	1.77	207	26.5	
		9.5	198	208	105	13.19	0.64	483	47	G-size break
		9.4	227	188	83	14.3	1.12	512	38.3	Clast Layer
		9.3	236	207	88	12.3	0.92	555	47.4	
		9.2	240	263	110	11.89	0.81	612	50.4	
		9.1	221	189	86	13.44	1.52	501	42.8	
		Clay (<4 µm)	Silt (4–63 µm)	V. Fine Sand (63–125 µm)	Fine Sand (125–250 µm)	Medium Sand (250–500 µm)		Coarse sand (500–1000 µm)		

The shadings corresponds to the grain-size.

versus cohesive forces (Baas et al., 2009, 2011, 2016). ‘Lower Transitional Plug Flows’ (*sensu* Baas et al., 2009) produce sub-parallel bands of muddy sand, overlain by low-amplitude bedwaves comprising isolated streaks of clayey-sand. Bedwave migration can form complex heterolithic stratification (Baas et al., 2016; Baker & Baas, 2020). In the field, these occur as ‘wavy morphologies’ (Hofstra et al., 2015, 2018). Therefore, both broadly linear and undulating bands can form under these transitional-flow conditions via tractional reworking beneath mud-laden transitional plug flows, as well as sandier ‘light bands’ (e.g. S3, Table 3) and muddier ‘dark bands’ (*sensu* Stevenson et al., 2020; e.g. S6, Table 3), depending on fluctuations in balance of turbulent versus cohesive forces. The distinctive ‘wave-like’ features described in bed type 1B (Material S1, Table 2) may correspond to the low-amplitude bedwaves of Baker and Baas

(2020), interpreted to form under upper transitional plug flows (Baas et al., 2009). Ripples formed overlying the banded interval (in BT 1A and 1B) may correspond to the ‘sandy current ripples’ of Baker and Baas (2020) forming under fully turbulent conditions. The requirement of prolonged traction suggests banded sandstones require slower deceleration rates compared to collapse of flows resulting in turbidites with linked debrites (Stevenson et al., 2020). Sheared dewatering features present at bed tops within both bed types 1A and 1B indicate turbulence damping and more rapid deposition (Stevenson et al., 2020). These beds are interpreted to reflect a more gradual deceleration during deposition of the flow head and body, followed by more rapid deceleration as the flow tail was depositing, possibly due to cohesive forces overriding reduced turbulence for the latter, creating a high rate of suspension fallout (Baas

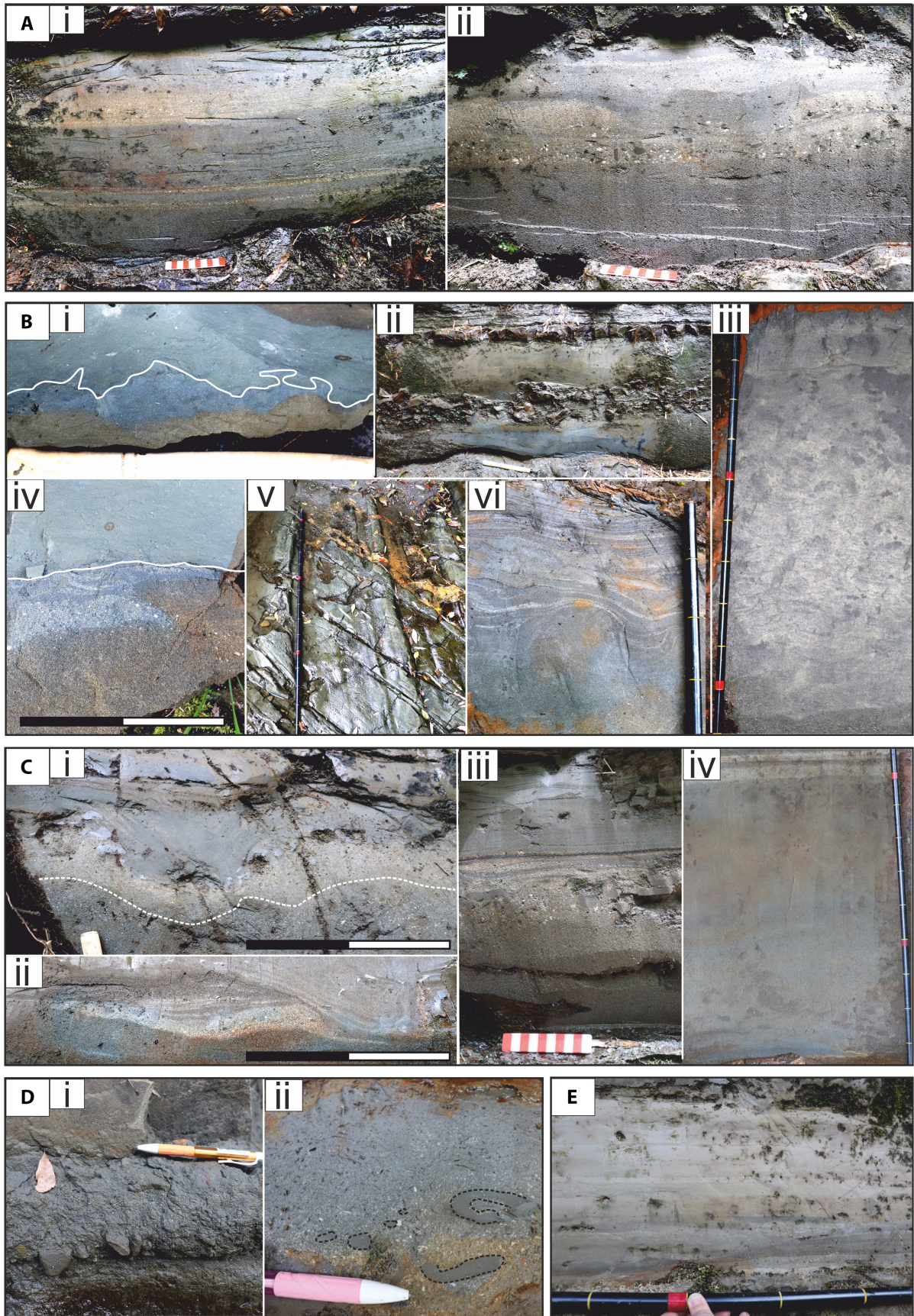


FIGURE 4 Representative photographs of bed types at location 2, descriptions in Table 1. (A) Bed type (BT) 1, banded beds consisting of banded siltstone, sandstone and gravel (Table 2), (i) bed type 1A, planar banded mudstone, sandstone and gravel layers, scale bar 10 cm. (ii) Bed type 1B, wave shaped bedforms consisting of mudstone, sandstone and gravel layers, scale bar 10 cm. (B) Bed type 2, hybrid beds, megabeds and bioturbated hybrid beds, (i) Bed type 2iC, lower sand-rich turbidite loaded into by upper mud-rich debrite with mm-cm mudclasts and organic matter, hammer handle at base for scale—25 cm long. White line indicates boundary between well sorted sandstone and debrite. (ii) Bed type 2iD, gravel and pebble wave shaped bedforms within sand-rich turbiditic component capped with mud-rich debrite; scraper for scale—30 cm long, (iii) bed type 2iF, dish structures within medium-coarse sandstone turbidite, scale bar shows 10 cm intervals, (iv) bed type 2iC, lower coarse sandstone turbidite sharply overlain by upper mud-rich debrite, scale bar shows 10 cm intervals. White line indicates boundary between well sorted sandstone and debrite. (v) Bed type 2iiG, grooves parallel to pole at the base of a megabed, scale bar shows 10 cm intervals, (vi) bed type 2iF, dewatered convoluted beds, scale bar at 10 cm intervals. (C) Bed type 3, low-density turbidites and high-density turbidites, (i) bed type 3I, diffuse banding (band separation marked by dashed white line) at top of bed overlain by a sharp grain-size break with mudclast layer and dewatered convoluted laminations, scale bar at 10 cm intervals, (ii) bed type 3K, discontinuously rippled sandstone with sharp, erosional and dewatered grain-size break to siltstone, scale at 10 cm intervals, (iii) bed type 3K, very coarse to gravel bed with mudclast layer and wavy laminations, sharp grain-size break to vf sandstone with organic rich bands and convolute laminations, scale bar 10 cm, (iv) bed type 3J, normal graded medium to fine grained turbidite with pumice bands at top, scale at 10 cm intervals. (Di) Bed type 4M, mudstone-sandstone debrite with burrows, (Dii) bed type 4M, mudstone to sandstone debrite with mm-cm clasts of organic matter and gravel to pebble mudclasts, burrows outlined by dashed black line. (E) Bed type 5N, layered ash and tephra bed, planar and undulating/erosional layers, organic material and burrows throughout

et al., 2009, 2011, 2016). Overall, this model fits well with the spectrum of bands seen in this study.

5.1.1 | BT 2

Bed type 2 (BT 2; sub-types C-F) is divided into three groups BT 2i- Hybrid beds, BT 2ii-Megabeds and BT 2iii-Bioturbated hybrid beds.

5.2 | BT 2i- Hybrid beds (Tables 2–4; Samples 1, 3, 4, 5, 7, 10, 11, 13)

Four sub-types of hybrid beds are recognised (C, D, E, F; Figure 4Bi-vi) that comprise bi-partite or tri-partite bed structures, with differences occurring within their sand-rich lower (and middle) divisions, while sharing a similar upper mud-rich division. H-divisions 1–5 are *sensu* Haughton et al. (2009).

Bed type 2iC description, lower division (H1 and H2): This type consists of relatively simple bi-partite beds, with a lower sand-rich division that is generally structureless, or normally graded, but can contain minor ripple or planar-laminations, or dish structures.

Bed type 2iC interpretation: The lower sand-rich division is interpreted as a turbidity current deposit due to normal grading with parallel and/or ripple-laminated top, diagnostic of layer-by-layer deposition from a non-cohesive flow. The variation in grain size and structures indicates deposition from both high and low-density turbidity currents (Lowe, 1982; Mutti, 1992).

Bed type 2iD description, lower division (H1 and H2): This bed type has the same bi-partite, sand-rich and mud-rich divisions, but with an intervening division of fine

sandstone and pumice, undulating crudely imbricated clast layers, grain-size breaks, dewatering structures including convolute laminations and mudstone-rich bands. Flutes and grooves are present at the base.

Bed type 2iD Interpretation: Grain-size breaks within beds represent a fluctuation of the flow from deposition to sediment bypass within a single event (Gladstone & Sparks, 2002; Kneller & McCaffrey, 2003; Stevenson et al., 2014a, 2015). This grain-size break is interpreted as a Type III surface (*sensu* Stevenson et al., 2014a), which is most common in proximal basin-floor localities. Dewatering structures are interpreted to form during an initial high rate of suspension fallout from a high-density turbidity current (Lowe, 1982). Convolute laminations form due to shear, buoyancy instabilities and/or water escape (Gladstone et al., 2018 and references therein), and indicate high suspension fall-out rates, deceleration of flows, and possibly interactions with local confining slopes (Tinterri et al., 2016). Baker and Baas (2020) demonstrated similar examples of lower hybrid bed divisions consisting of a mix of sandstone-mudstone rather than the homogeneous structureless sandstone of Haughton et al. (2009). Planar and undulating mudstone-rich bands present within the top of the lower division are interpreted to form under these transitional-flow conditions via tractional reworking beneath mud-laden transitional plug flows (Baas et al., 2016; Stevenson et al., 2020) depending on fluctuations in the balance of turbulent versus cohesive forces. The muddier interval may have been formed by a cohesive flow that decelerated comparatively more slowly, and which generated sub-parallel banding (Baas et al., 2016; Stevenson et al., 2020). See BT 1 for further discussion. Crudely imbricated, angular, mudclast layers up to pebble in size, are interpreted to form by either (i) deceleration of a basal dense flow followed by the bypass of a turbidity

current reworking clasts, creating tractional structures, or (ii) by direct deposition of bedload transported clasts, with the angular nature suggesting travel distances were short (Baas et al., 2021). In both cases, the sharp grain-size break above the clast-layer indicates subsequent full bypass of the flow down-dip. Flute marks are interpreted to have been caused by erosive, turbulent eddies at the base of the flow. Groove formation is discussed below. Clasts at the base of, and throughout, beds were sourced from erosion and entrainment of the weakly consolidated underlying substrate, resulting in the sharp surfaces at the base of the turbidite component.

Bed types 2iE and 2iF description: Similar sand-rich divisions (H1) are noted in bed types 2iE and 2iF (their middle division, Material S1, Table 2), but in these cases, a 10–40 cm lower division can be present containing 80% clasts-by-volume. The lower, mudclast-dominated section displays an internal clast-supported texture. Clasts are intraformational, sub-angular to sub-rounded, randomly orientated, and range in size from granule to boulders with long axes up to 30 cm. Flutes, rare scours and rare grooves are found at the base.

Interpretation: the sand-rich divisions are unlikely to have formed by a traction carpet due to the large size of clasts compared to the thickness of the layer (clasts are typically less than a tenth of the thickness of the traction carpet; Sohn, 1997). These are interpreted as the product of eroded mudclasts that have been transported as bedload, or were deposited from flows via competence-driven deposition. A bedload interpretation is supported by the abraded nature of these intraformational mudclasts (sub-angular to sub-rounded) and the presence of clast sizes up to boulders. The random orientation and lack of imbrication suggests that they accumulated as a result of overpassing (large clasts rolling over a finer substrate; Allen, 1983) rather than moving as a bed-covering traction layer. Granules and other finer components may also have accumulated from competence-driven deposition. Grooves present at the base of the sand-rich middle division (BT 2iE and 2iF, Material S1, Table 2) may be caused by a fore-running debris flow, which would have sufficient cohesion to hold a clast in suspension and drag it across the substrate (Baas et al., 2021; Peakall et al., 2020).

Description, upper division 2iC-F: The upper division of all four hybrid bed sub-types (Material S1, Table 2) is an argillaceous-matrix that supports chaotically distributed larger clasts (H3). The clasts comprise mudstones and pumice (millimetre to 1 cm diameter), and organic matter and shelly fragments (millimetre to 1 cm diameter). Commonly, the upper division is foundered or loaded into the lower division.

Interpretation: The upper divisions are interpreted as a debrite formed by inefficient sorting and *en masse* deposition from a cohesive flow. Mudstone and pumice clasts were

likely sourced from up-dip deposits, while organic matter and shelly fragments likely originated from the up-dip shelf. Foundering and load structures at the base of this division formed due to rapid deposition and buoyancy instabilities, indicating that deposition of the debris flow took place soon after deposition of the antecedent turbidite. Debrites such as this can form due to partial flow transformation as a turbidity current traverses the slope, so that the subsequent incorporation of mud and mudclasts damps flow turbulence (Haughton et al., 2003; Talling et al., 2004). Cohesive ‘freezing’ of debris flows can cause an undulating sharp top surface. Hybrid beds have been previously considered as uncommon in proximal fan settings (Hodgson, 2009), but they have been documented in channel-fills and CLTZs due to enhanced erosion of underlying substrate (Baas et al., 2021; Brooks et al., 2018a; Ito, 2008; Kane et al., 2010; Mueller et al., 2017; Terlaky & Arnott, 2014).

5.3 | BT 2ii- Megabeds (Tables 2–4; Sample 8)

Bed type 2ii encompasses seven megabeds that are 2.4–4.1 m thick (bed sub-type G; Figure 5) which due to their thickness are designated as a sub-category of hybrid beds.

Description: These beds contain many of the same features as the hybrid beds described above, but what are several beds in one location, can be traced laterally over a few metres to tens of metres, into a single amalgamated unit (Figure 5A,B). This bed type shows marked scouring at the base of beds, boulder-sized clasts, ductile deformation structures and preservation of internal structures within ripped-up amalgamated beds.

Interpretation: The boulder-sized clasts and ripped-up beds with preserved internal structures that are contained within the amalgamated beds indicate very high-energy processes, and local sources for the entrained material (e.g. Figure 5Bv). Ductile deformation structures indicate the substrate was partially consolidated rather than lithified prior to erosion (Figure 5A). The variation in the amount of lateral disarticulation over several metres indicates abrupt changes in processes from deformed to undeformed sections (Figure 5A). These megabeds are interpreted as packages of other bed types. They mostly consist of hybrid beds (BT 2i) and some banded beds (BT 1) that were remobilised as slides, slumps and debris flows, either locally or further upslope. As these remobilised deposits are transported downslope, they continue to entrain substrate material as evidenced by the erosion and scouring at the base of beds.

The extensive ripped-up clasts made up of whole packages of beds (shown in the example in Material S1) show

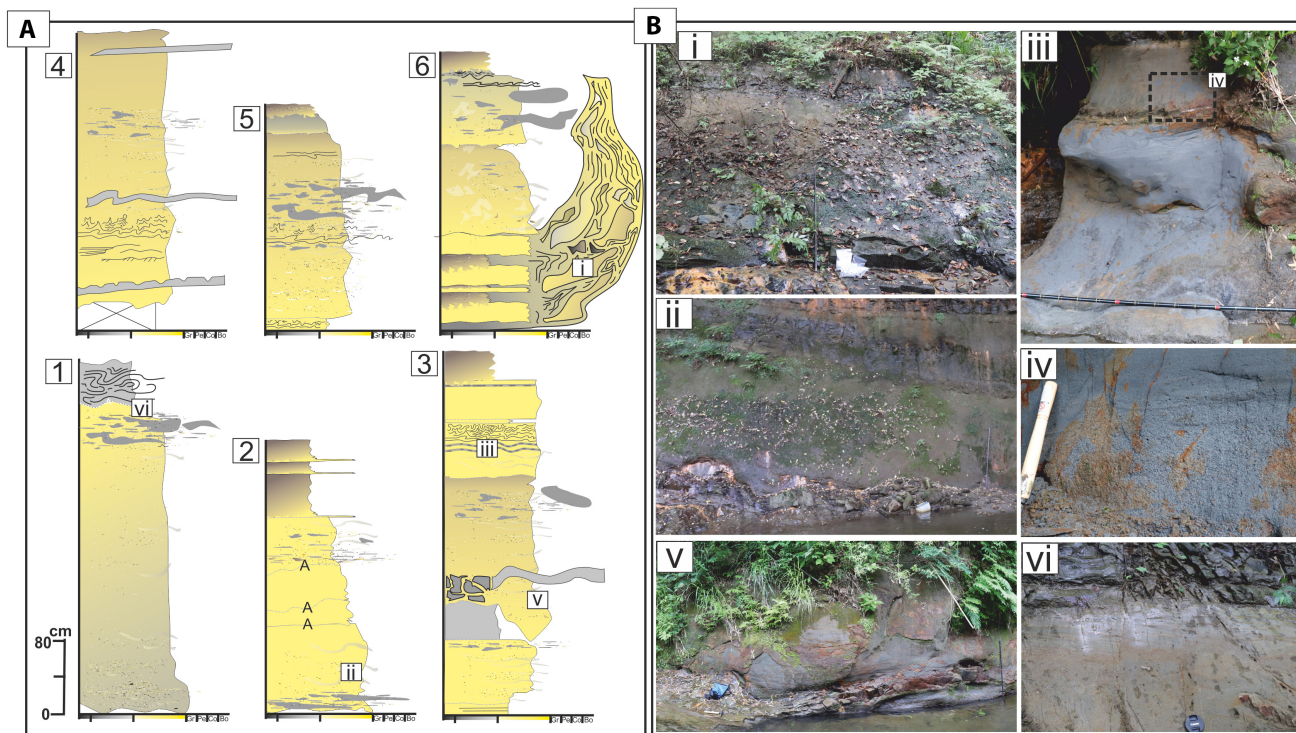


FIGURE 5 (A) Sketch logs of megabeds at location 2, bed type 2, group 2ii, for description see Table 2, for location within section see Figure 6, roman numerals relate to photographs in B, (B) photographs of megabeds see A for location within bed. See Figure 6 for key to logs, A—denotes amalgamated bed contacts

similarities with Type 1 beds of Cunha et al. (2017), which are interpreted as reflecting the sudden deceleration of dense flows, producing flow impacts and hydraulic jumps (see also Tinterri et al., 2016). Large ripped-up beds may be formed by similar processes as HEB1 beds of Fonesu et al. (2018) in the Gottero Formation, Italy, which are interpreted to form due to rip-up of rafts from underlying substrate and subsequent disaggregation.

5.4 | BT 2iii- Bioturbated hybrid beds (Tables 2–4; Sample 14)

Bioturbated hybrid beds are a specific type of hybrid bed that have a moderate degree of bioturbation throughout both the lower and upper division (bed sub-type H, BI index 2–3, after MacEachern et al., 2005).

Description: These beds are thinner (0.3–1 m), with minor basal erosion, and better sorted than the other hybrid bed groups described above. Burrows are both vertical and horizontal, isolated and cross-cutting, millimetres to 3 cm in diameter and 2–20 cm long; they are present in the lower sand-rich division. Mudstone bands, both planar and undulating, are present towards the top of the lower sand-rich division. The upper division has an argillaceous matrix, with millimetre to 1 cm chaotically distributed clasts of mudstone and pumice, along with

similar sized organic matter and shelly material; this division may show foundering and loading at its base.

Interpretation: Due to the thinner bedding, better sorting and less erosion these beds are interpreted as lower energy flows than the previous hybrid bed types. The presence of *Thalassinoides* and *Planolites* in these beds along with *Zoophycos*, *Chondrites* and other ichno-fauna recognised by Ito (1998a), suggest a palaeowater depth of ca 400–1500 m (Baba, 1990; Kitazato, 1989). The moderate degree of bioturbation (BI 2–3) of these beds indicates sufficient energy for nutrients and oxygen to be delivered from the shelf, but also for energy to be low enough for many organisms to be able to burrow and feed. As these bioturbated hybrid beds are interpreted as two portions of the same flow, it is possible that the burrowing organisms were brought down within the turbidity current to rapidly colonise the beds. Moreover, the layer-by-layer deposition of the basal turbidite may have allowed time for burrowing organisms to move up through the beds creating the burrowing networks noted in Table 2/Material S1 immediately after or during deposition of the bed, whereas the relatively quicker *en masse* deposition of the overlying debrite would not allow the organisms to escape upward, making extensive burrowing less common.

Planar and undulating mudstone bands present within the top of the lower turbidite (H1) division are interpreted as having formed under transitional-flow conditions via

tractional reworking beneath mud-laden transitional-plug flows (Baas et al., 2016; Stevenson et al., 2020). The muddy consistency may have been formed by a cohesive flow that decelerated comparatively slowly compared to the structureless portion of the bed, generating sub-parallel banding (Baas et al., 2016; Stevenson et al., 2020). See BT 1 for further interpretation.

The upper division is interpreted as a mud-rich debrite due to the argillaceous matrix supporting chaotically distributed larger components (millimetres to 1 cm), which indicate an inefficient sorting associated with *en masse* deposition from a cohesive flow. The clast sizes (millimetres to 1 cm) suggest that this debrite was deposited by a low-strength debris flow, as defined by Talling et al. (2012). Mudstone clasts and pumice were likely sourced from underlying up-dip deposits, and the organic matter and shelly material from the up-dip shelf. Foundering and load structures at the base of this division formed due to rapid deposition and buoyancy instabilities, indicating that the deposition of the debris flow took place soon after deposition of the turbidite (Lowe, 1975).

5.5 | BT 3—Low-density and high-density turbidites (Tables 2–4; Samples 2, 9, 12)

Description: Bed type 3 consists of poorly sorted conglomeratic to finer-grained sandstone beds, with erosional bases with scours, rare grooves and flutes, the latter filled with coarse sand/gravel lags. The beds grade normally to very fine sandstone and siltstone with ripple, climbing ripple, parallel and convolute laminations. Layers of crudely imbricated mudstone clasts can be present within the beds, sometimes forming wavy bedforms. The thickness of BT 3's very fine-grained to gravel-grade beds varies between 0.2–1.2 m (sub-types I, J, K, L; Figure 4 Ci–iv). See Material S1 for full description.

Interpretation: The erosional basal bed surfaces indicate high-energy flows that entrained substrate, forming scour features prior to deposition. Flutes are filled with coarse sand/gravel lags (0.6–4 mm), representing a transient bypass surface (Kuenen, 1953, 1957), similar to Type I surfaces of Stevenson et al. (2014a). Flute marks are interpreted to have been caused by erosive turbulent eddies at the base of the flow, whereas the grooves were formed by large clasts transported at the base of a cohesive flow component, such as a forerunning debrite (Baas et al., 2021; Peakall et al., 2020). Normal grading within beds indicates layer-by-layer deposition from a waning turbulent flow. Grain-size breaks within the bed are indicators of sediment bypass (Gladstone & Sparks, 2002; Kneller & McCaffrey, 2003; Stevenson et al., 2013), and represent a fluctuation of the flow from deposition to bypass within a

single event, with angular clasts indicating a local source and therefore local erosion. The layers of crudely imbricated clasts are interpreted to form by the reworking of lag deposits and the subsequent imbrication of their clasts in the direction of flow. This would occur during either multiple pulsed events within one flow, or several separate flows; either of which suggests that significant bypass occurred. Climbing ripples are interpreted to have formed from continuous bedload traction under high-aggradation rates (Allen, 1970; Jobe et al., 2012; Morris et al., 2014). Convolute laminations are interpreted to have formed due to shear, buoyancy instabilities, and/or water escape (Gladstone et al., 2018 and references therein), and indicate high suspension fall-out rates.

5.6 | BT 4—Debrites

Description: Bed type 4, sub-type M (Material S1, Table 2), is characterised by poor sorting, a lack of sedimentary structures (Figure 4Di–ii), and gravel-sized to boulder-sized mudstone clasts throughout. See Material S1 for full description.

Interpretation: Bed type 4 examples are interpreted to have been deposited *en masse*, under laminar-flow conditions, by intermediate to high strength debris flows (*sensu* Talling et al., 2012). Erosive undulating bases indicate a high-energy flow that scoured the underlying substrate. Ductile deformation structures within mudclasts indicate that the substrate was partially consolidated rather than lithified prior to erosion. Sharp, undulating bed tops formed due to cohesive 'freezing' of debris flows (i.e. Lowe, 1982). Intense bioturbation of bed tops indicates the development of a nutrient-rich, well-oxygenated environment, in a state of quiescence immediately after the bed deposition. A mixed foraminiferal assemblage typical of the upper and middle bathyal zones has been documented in bed type 4 by Ito (2008).

5.7 | BT 5—Ash/Tephra

Description: Bed type 5, sub-type N (Material S1, Table 2; Figure 4E) consists of finer-grained ash with some intercalated siltstone, organic matter, pumice and scoria with minor low-angle cross-laminations. These form uniform drapes across the basin, and therefore can be used as correlation datums.

Interpretation: These beds are interpreted as ash-fall from numerous volcanic eruptions, which occurred throughout the Pleistocene in the Japanese islands (Ishiwada et al., 1971; Ito, 1994, 1995; Mitsunashi, 1961; Mitsunashi et al., 1959). Intercalated pumice and scoria are interpreted as tephra from explosive eruptions. Organic

and siliciclastic material has been incorporated into the volcanic deposits, by low-density turbidity currents and bottom currents that were active during deposition. Low-angle cross-laminations observed in these deposits may be similar to low-amplitude bedwaves (Baker & Baas, 2020), which are interpreted to have formed by lower and upper-transitional plug flows that contained varying proportions of sand and mud. These types of flows have a high yield strength and reduced turbulence at the base, which limits the bedforms to long, thin shapes, producing low angle cross-lamination (Baas et al., 2016; Baker & Baas, 2020).

6 | CLASSIFICATION AS A CLTZ

The precise palaeoenvironmental setting is challenging to constrain, and could record a channel mouth or proximal lobe setting. For instance, the classic example of a CLTZ from the Navy Fan (Normark et al., 1979) was later discovered with higher resolution side-scan sonar data (Carvajal et al., 2017) to be a downstream widening, and shallowing channel-mouth transition zone. Despite this, the regional setting at the base-of-slope (Ito, 2008), with channel levee deposits up-dip and medial to distal lobes down-dip, together with the recognition of scour-fills, grain-size breaks, sand-rich hybrid beds and rip-up clasts and grooves (suggesting bypass of forerunning debris flows down-dip; Baas et al., 2021; Peakall et al., 2020) supports a sediment bypass-dominated setting (Brooks et al., 2018b) and interpretation of a CLTZ (Ito, 2008). Moreover, a mixed-foraminiferal assemblage that has previously been recorded in the debrites is dominated by species typical of the upper and middle bathyal zones (1000–1500 m palaeowater depth) similar to faunas in interbedded hemipelagites (Ito, 2008). Furthermore, the zone in this study does appear to fall broadly within the original definition of a CLTZ by Mutti and Normark (1987, 1991) and Wynn et al. (2002b) as ‘the region that, within any turbidite system, separates well-defined channels or channel-fill from well-defined lobes or lobe facies’.

7 | DEPOSITIONAL STAGES

The logged succession was classified into three distinct stages (1, 2 and 3 outlined below) based on: the mudstone to sandstone ratio; the thickness of beds; variations in the proportions of bed types described above; the changes in depositional architecture; and the presence or absence of scouring and erosion (as well as other bypass indicators). These are summarised in Table 5. Stage 2 is separated into three packages, which each show a repeating pattern up-section of similar bed types and architecture changes.




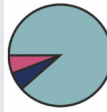

7.1 | Stage 1

Stage 1 contains a significant proportion of mudstone (sand-to-mud ratio of 55:45) compared to the later stages, as well as the lowest average bed thickness of 43 cm (Table 5). This stage primarily comprises hybrid beds (BT 2i) and banded beds (BT 1), as well as a few low-density turbidites to high-density turbidites (BT 3; Figure 6). The O16 ash marker bed is documented at the top of this stage (Figure 6), and was correlated throughout the region (Ishiwada et al., 1971; Ito, 1994, 1995; Mitsunashi, 1961; Mitsunashi et al., 1959). Overall, palaeocurrent readings obtained from ripples, grooves and flutes are consistently towards the north-east (Figure 6). Beds deposited during this stage are fairly tabular, with most extending laterally for tens of metres, with only minor changes in thickness, and a few thin beds that are eroded-out laterally (Figure 7). Scouring at the base of, and within beds, is common but scour depths do not exceed 20 cm, and they are generally less than a few centimetres deep. The majority of beds comprise relatively thin (<50 cm thick) hybrid beds which have muddy debritic caps (Figure 6), indicating up-dip erosion and rapid flow deceleration. These hybrid beds are interbedded with banded beds (BT 1), which only occur in Stage 1, and are interpreted to be formed by transitional clay-rich flows that are cohesive, and likely decelerated relatively slowly (Baas et al., 2009; Stevenson et al., 2020). Another feature only observed at Stage 1 are tens of centimetres thick reworked-lag deposits, which also support up-dip substrate erosion as well as prolonged periods of sediment bypass (e.g. S4, Table 3).

The presence of scouring, mudclast lags and hybrid beds in Stage 1 all indicate some high-energy erosive and bypassing flow conditions at this location, supporting an active CLTZ. Sandstone banding in Stage 1 beds indicates that some of the flows experienced slower deceleration rates (Stevenson et al., 2020), suggesting either more flow variability compared to Stages 2 and 3, or that the break-in-slope was more gentle at this early stage.

In previous studies, this interval was interpreted to represent relatively low-energy conditions and to have therefore developed during a relative sea-level highstand (Ito, 1998b), with few large flows traversing the slope to the basin-floor. However, due to the evidence presented in this study of erosion and bypass, this stage may have formed during higher energy conditions than previously suggested, and is therefore interpreted to represent the transition from a highstand systems tract to a falling-stage systems tract, as local relative sea level began to fall. Furthermore, this stage may have been deposited during an initial phase of lobe initiation and building, with the bulk of flows forming lobe deposits in down-dip locations (Ito, 2008).

TABLE 5 Thickness information, numbers of beds and bed type information on Stages 1–3 for location 2 (CLTZ) and for corresponding up-dip location 1 (see Figure 8), see text for details. Key for bed-type distributions displayed below, 'L-H' for 'low to high' density turbidite beds

Location 2 (CLTZ)										Location 1 (UP-DIP)				
Stage	Thickness	No. of beds	Average bed thickness	Sand:Mud	Bed types distribution	Scouring	Other	Thickness	No. of Beds	Average bed thickness	Sand: Mud	Other		
1	12.8 m	30	0.43 m	55:45		Low depth, infrequent, <20 cm deep	Reworked lags, grain-size breaks	>5 m (not complete section)	>11	0.45 m	58:42	Tabular beds, planar laminated		
2.1	17.4 m	17	1.02 m	79:21		Medium to high, frequent, >1 m	Grain-size breaks, megabeds, lateral discontinuity	24.8 m	15	1.65 m	96:4	Megabeds, amalgamated, frequent scouring		
2.2	31.2 m	19	1.64 m	81:19		Very high, frequent, up to several m's	Megabeds, lateral discontinuity	36 m	26	1.38 m	90:10	Debrites, megabeds, lateral discontinuity, frequent scouring		
2.3	13 m	18	0.72 m	71:29		Medium, frequent, >1 m	Minor bioturbation, megabeds, lateral discontinuity	17 m	21	0.81 m	82:18	Debrites, remobilisation, tabular mud-rich beds, minor scouring		
3	15.9 m	31	0.51 m	60:40		None	Significant bioturbation, very tabular beds	14 m	17	0.82 m	66:34	Debrites, Megabeds, more tabular than 2.2–2.3 Infrequent scouring		

KEY: Bed Types:  1: Banded beds;  2ii: Megabeds;  2iii: L-H density turbidite beds;  3: Ash/Tephra beds;  4: Debrite beds;  5: Hybrid beds;  2i: Bioturbated hybrid beds;  4: Debrite beds.

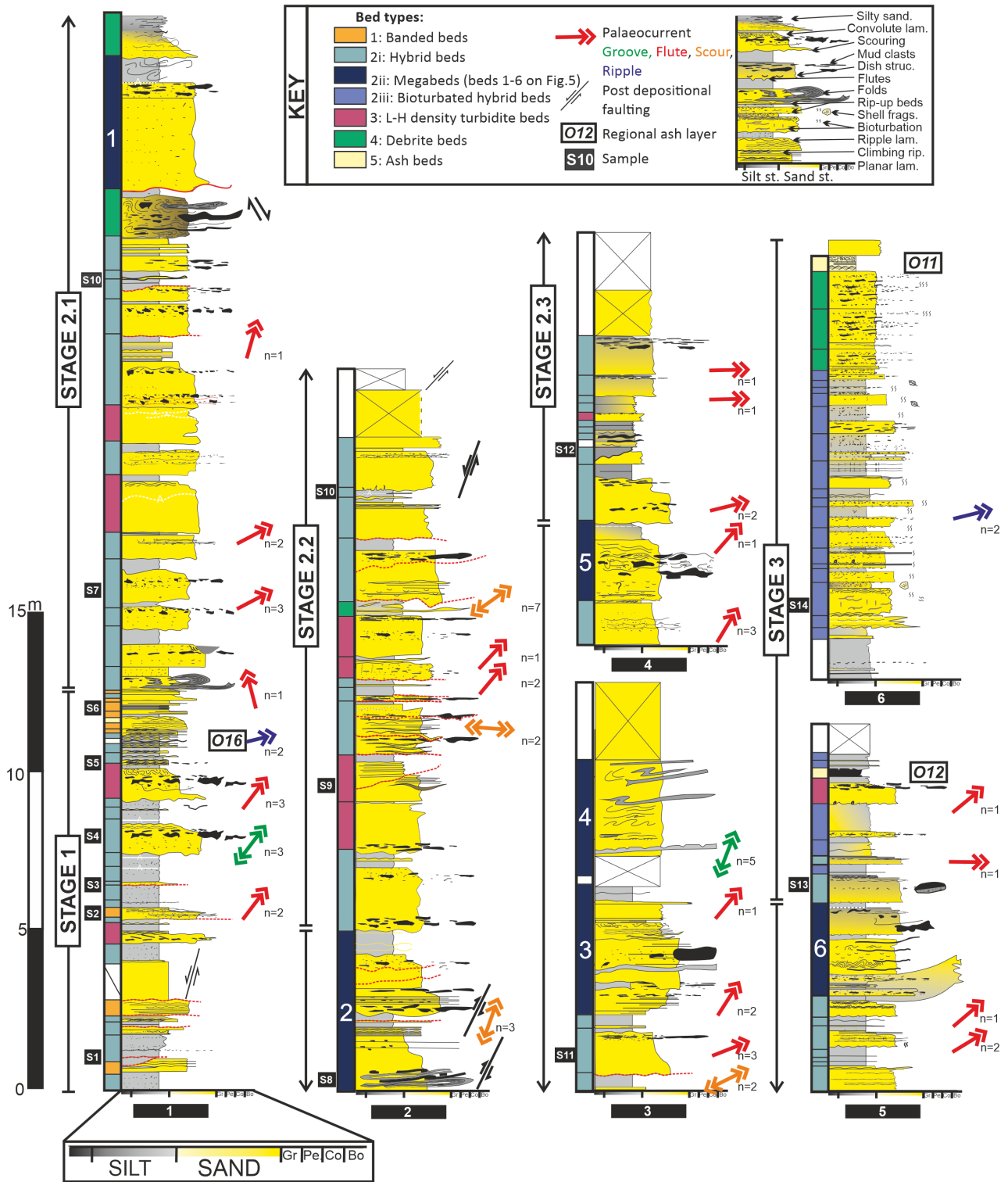


FIGURE 6 Sketch of logged section at location 2, over 100 m in total. Location of section shown in Figure 3A,C. Less detailed log of same section with above and below stratigraphy shown in Figure 2C. Column of colours on the left indicates facies group. Arrows indicate averaged palaeoflow direction with $n = X$ indicating number of measurements. Photographs of each stage are shown in Figure 7. More detailed sketches of megabeds shown in Figure 5, numbers of megabeds correspond to numbers in Figure 5A. Bidirectional scour palaeocurrents were taken from scour margins, unidirectional scour measurements were taken from smaller tens of centimetres width and length scours with megaflute like morphology (Brooks et al., 2018a fig. 12F) where flow direction could be noted.

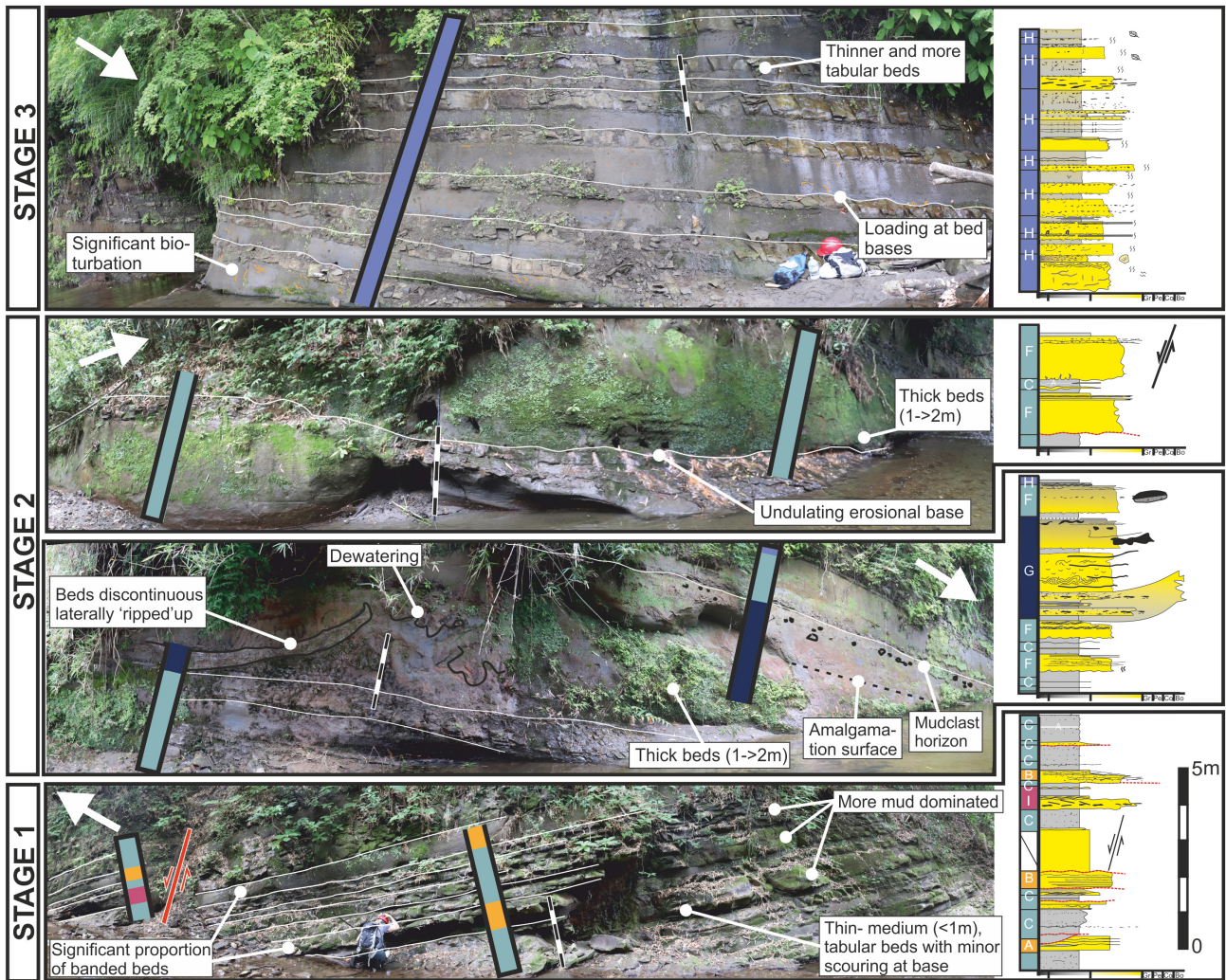


FIGURE 7 Photographs of stages 1, 2 and 3, showing the architecture of beds and facies groups at location 2. Logs correlate to section shown in photograph. See text for descriptions of each stage. Statistics for each stage shown in Table 5. Key to logs and facies colours shown in Figure 6. Refer to Table 2 for corresponding descriptions of bed sub-types A–H. Palaeocurrents are from combined ripples and sole structures i.e. flutes, grooves and scours

7.2 | Stage 2

Stage 2 is sub-divided into three packages (Package 1, 2 and 3 from base to top) based on a distinctive bed type distribution expanded on below. Overall, this stage is dominated by sandstone (sand-to-mud ratio 77:23), and each of the three packages contains a very similar number of beds (Table 5; Figure 7). Each package consists of hybrid beds interbedded with minor turbidites (BT 2i and 3), with the top of the package capped with one or two megabeds (BT 2ii) with intervening debrites (BT 4; Figures 6 and 7). Overall, beds in Stage 2 are less tabular than in Stages 1 and 3, and with more erosive scoured bases (up to 1 m deep) and undulating tops. The beds can be laterally discontinuous, and their thickness can change by several decimetres over short (tens of metres) distances.

7.3 | Package 1

Package 1 is 17.4 m thick and consists of 17 beds (Table 5, Figures 6 and 7), which are primarily hybrid beds (BT 2i) with minor turbidites (BT 3), capped by two megabeds (BT 2ii), which are themselves interbedded with a debrite (BT 4). The average bed thickness (1.02 m) is more than twice that of Stage 1, and the sand-to-mud ratio is markedly higher (79:21, Table 5). Package 1 records an overall thickening-upwards trend, along with an increasing scour depth (up to 1 m deep and 1.5 m in width), and size/volume of mudclast inclusions. No bioturbation is recorded in Package 1. Palaeocurrents that were measured from flute casts indicate a transport direction towards the north–north-west at the base and north-east and north–north-east in the mid-package. Scour palaeocurrents are towards the north–north-east in the upper part of the package (Figure 6).

Erosion surfaces and grain-size breaks, which are present throughout, indicate that flows were bypassing the area and continuing down-dip (Stevenson et al., 2015). Overall, Package 1 is interpreted to represent a high-energy environment, dominated by high-density turbidites with or without co-genetic debritic caps. These are interpreted to have been deposited in an environment with significant variation in flow conditions, fluctuating between rapid deposition, bypass and erosion. An increase in erosion-surface frequency and depth indicates an increase in sediment bypass. This is topped with a bundle of megabeds and debrites, which indicate remobilisation, and may be diagnostic indicators of slope instability.

7.4 | Package 2

Package 2 (31.2 m thick) consists of 19 beds (Figures 6 and 7) and is similar to Package 1 in bed type distribution (Table 5). The average bed thickness (1.64 m) shows a continued increase from Package 1, along with a slight increase in the sand-to-mud ratio (81:19). The thickest beds are present at the top of the section, but an overall thickening-upward trend is not as distinct as in Package 1. Package 2 also includes scour surfaces (up to 50 cm deep, and 1.5 m wide) and a higher size/volume of mudclast inclusions towards its top. This occurs along with a higher number and depth of erosion surfaces, as well as more common grain-size breaks (Figure 6). Very minor bioturbation is noted within the interbedded siltstones. The orientation of scour margins are *ca* east to west, or (in exposures with 3D constraint) show a north-east palaeoflow direction. Palaeocurrents from flutes indicate a transport direction towards the north-east in the lower-mid package. In the upper package, flutes continue to indicate a palaeoflow direction towards the north-east; while grooves display a north–north-east to south–south-west orientation (Figure 6).

The increase in mudclasts, scours and erosion surfaces up-section, indicates an increase in erosion and bypass combined with increased slope instability, all of which is evidenced by the megabeds at the top of section. The presence of bioturbation within the package suggests either a more hospitable environment for burrowing organisms, or potentially increased time between flows for burrows to be established.

7.4.1 | Package 3

Package 3 (13 m thick) consists of 18 beds made up of similar bed types to Packages 1 and 2 (Figures 6 and 7) but with a higher proportion of hybrid beds (BT 2i), and no debrites (BT 4) present (Table 5). Package 3 displays a

decrease in sand-to-mud ratio (71:29), and decrease in average bed thickness (72 cm), both with respect to the two underlying packages, making this the most mud-prone package of the overall sand-dominated Stage 2. Minor bioturbation is recorded in some beds (BI 1–2). Flutes indicate a palaeoflow direction towards the east in the lower/mid sections of Package 3, while they indicate a north-east palaeotransport direction in the upper part of the package (Figure 6). The frequency/depth of scour surfaces increases up section (up to 50 cm deep, 1.5 m wide).

7.4.2 | Stage 2 summary

The regional setting at the base-of-slope (Ito, 2008), associated with the recognition of: discontinuous beds; scour-fills; grain-size breaks; sand-rich hybrid beds; rip-up clasts; along with the thick-bedded sand-rich nature, support an interpretation that Stage 2 represents deposition in a CLTZ to proximal lobe environment during high sediment input and high-energy flow conditions (Brooks et al., 2018a). The bioturbation suggests periods suitable for burrowing organisms to begin bed colonisation. In previous studies, this stage was interpreted to have developed as relative sea level continued to fall and reached a low-stand (Ito, 2008). This is consistent with the finding of this study, with Stage 2 constituting the bulk of sediment input and lobe building.

7.5 | Stage 3

Overall, Stage 3 (15.9 m thick) is less sand-rich than Stage 2 (sand-to-mud ratio 60:40) and comprises 31 beds with a marked decrease in average bed thickness (0.51 m), and change in bed types from Stages 1 and 2 (Figures 6 and 7). Two ash beds are documented in this interval: O12 near its base and O11 at its top (Figures 4E and 6), both of which have been correlated throughout the region (Ishiwada et al., 1971; Ito, 1992, 1994, 1995, 1998a, 1998b; Mitsunashi, 1961; Mitsunashi et al., 1959). Bioturbated hybrid beds (BT 2iii) that are tabular at outcrop scale dominate Stage 3. Beds have frequent, but small (<6 cm) loads at bed bases. Flutes indicate palaeotransport direction to the east and north-east (Figure 6), with no major scouring recorded throughout this stage. Very few palaeocurrents are recorded throughout the mid and upper parts of Stage 3, with a few ripple cross-lamination measurements towards the east–north-east (Figure 6). The top of the section comprises 5 m of debrites, indicative of another period of slope instability. These debrites are matrix-supported, with rounded mudclasts and high amounts of bioturbation in both the upper portion of beds and on top

surfaces (BI 3–5; [Figure 4Di](#)). This signifies that they were deposited with sufficient time between each event for organisms to significantly colonise the substratum, or the organisms were brought down-slope within the flow.

With limited banding, lags, scour-fills or grain-size breaks, together with the more tabular, highly bioturbated beds (BI 3–5), Stage 3 contrasts markedly with underlying Stage 1 and 2. Because of the reduction in average bed thickness with respect to the underlying unit, significant increase in bioturbation, and a lack of evidence for substantial sediment bypass and scouring, Stage 3 is interpreted as a lower-energy environment than Stage 2. The increased tabularity of beds may support deposition in a lobe environment (Prélat et al., 2009), with the sand-to-mud ratio and facies consistent with an interpretation of an off-axis lobe setting (Prélat et al., 2009; Spychala et al., 2017a).

Stage 3 has been previously interpreted as the start of the transgressive systems tract during initial relative sea-level rise (Ito, 2008), where O12 was deposited slightly prior to the onset of the subsequent transgression, while O11 was deposited at a more advanced stage of the transgression. The onset of the transgression might have occurred slightly earlier than previously envisaged, given the upward fining trend that characterises Stage 3, which recorded the transition to a lower energy and more consistently ordered lobe development. This was associated with reduced levels of scouring, as sediment input diminished, albeit some initial slumping occurred, potentially caused by re-equilibrium of the slope.

7.6 | Comparison to up-dip section (Location 1)

A less detailed logged section located 4.5 km palaeogeographically up-dip on the former continental slope (Location 1 of Ito, 2008; [Figure 8](#)) shows many similarities with the section described above ([Table 5](#)). Ash beds O16, O12 and O11 have been used for correlation between sections, with O16 used as a datum ([Figure 8](#)). Location 1 displays the same tripartite Stage 1–2–3 construction as Location 2. The overall change from more mud-rich beds (Stage 1) through sand-rich (Stage 2) to mud-rich (Stage 3) can generally be recognised in up-dip Location 1, as well as other up-dip and down-dip sections in the area (see Ito, 2008 for details). Key differences in this up-dip section include the presence of thicker, more amalgamated and remobilised beds in Stage 2 and Stage 3 ([Table 5](#)), interpreted as channel-collapse deposits, due to the proximity to up-dip channels (Ito, 2008), as well as a marked decrease in hybrid beds. Packages 1, 2 and 3 of Stage 2 at Location 2 can be crudely correlated

up-dip to Stage 2 at Location 1 ([Figure 8](#)), but beds are more amalgamated and do not show the distinctive presence of megabeds at the top of each sub-package, only the debrites. The up-dip Location 1 section shows less evidence of bypass including fewer scour-fills, fewer grain-size breaks and fewer discontinuous beds than the Location 2 section. Consequently, the Location 1 section is interpreted to have formed outside the CLTZ in an up-dip channel complex (Ito, 2008, [Figure 9](#)). Hybrid beds are present but sporadically distributed within the up-dip Location 1 section, while they are dominant down-dip at Location 2. Past studies have shown that hybrid beds are present further down-dip (roughly 8 km; Ito, 1998b, 2008), but are also sporadically distributed spatially and through the section, with the most hybrid bed-rich strata being found at Location 2.

8 | DISCUSSION

8.1 | Development of hybrid bed-rich and thick CLTZ stratigraphy

A high proportion of hybrid beds are preserved in this base-of-slope setting compared to base-of-slope settings in other studies (Brooks et al., 2018a; Hofstra et al., 2015; Pemberton et al., 2016; Van der Merwe et al., 2014). Hybrid beds develop through flow transformation following significant entrainment of a muddy substrate and/or declining turbulent energy (Amy & Talling, 2006; Haughton et al., 2003, 2009; Hodgson, 2009; Lucchi & Valmori, 1980; Muzzi Magalhaes & Tinterri, 2010; Southern et al., 2015), and are commonly observed within the distal fringes of lobe systems (Fonnesu et al., 2018; Haughton et al., 2003; Hodgson, 2009; Kane & Pontén, 2012; Kane et al., 2017). Recently, studies have shown that hybrid beds can also develop in base-of-slope settings (Baas et al., 2021; Brooks et al., 2018a; Fonnesu et al., 2018; Ito, 2008; Mansor & Amir Hassan, 2021), and are generally associated with frontal lobes (Mueller et al., 2017; Spychala et al., 2017a, 2017b, 2021). The stratigraphic distribution of hybrid beds has been linked to the character of the supply slope and seafloor relief, where hybrid beds are invoked to develop during periods of disequilibrium in out-of-grade slopes (Haughton et al., 2003, 2009; Hodgson, 2009; Pierce et al., 2018; Spychala et al., 2017a, 2017b). Therefore, they are dominantly deposited during stages of fan initiation and growth (Kane & Pontén, 2012; Privat et al., 2021), or up-dip erosion during spatial expansion at the CLTZ (Brooks et al., 2018a). The equilibrium state of the slope is important, as when a system is above-grade (Prather, 2000, 2003) flows preferentially erode the slope to form a profile that is at equilibrium. Consequently, the availability of mud-rich

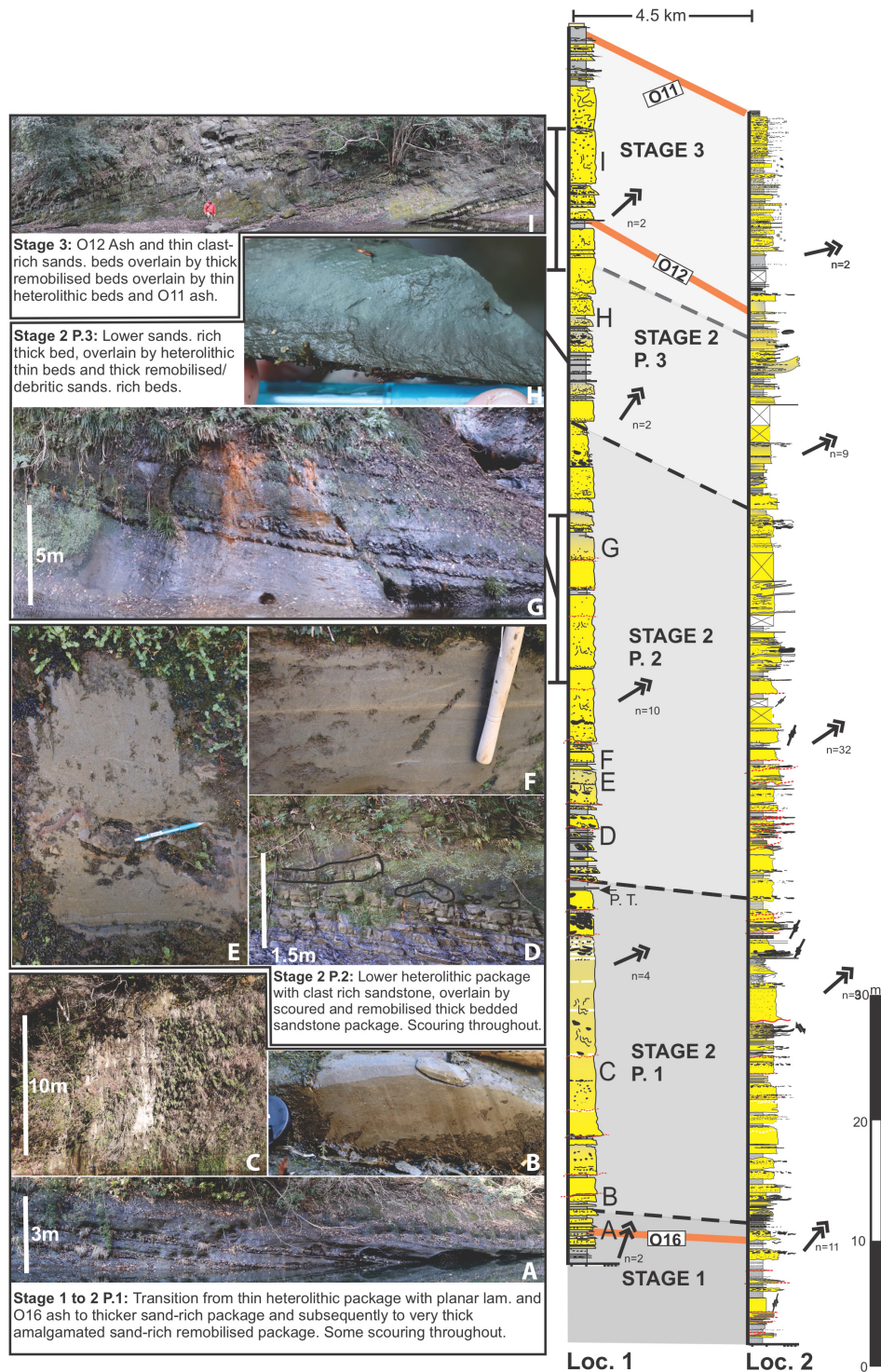


FIGURE 8 Comparison of main study section (location 2, Ito, 2008) and updip location 1 (Ito, 2008). See Figure 3 for geographical context. (A) Stage 1 thin bedded section with O16 ash and minor scouring, similar to stage 1 in downdip section. (B) Thin debritic bed, with grooves at base towards NE. (C) Thick bedded sandstone package. (D) Thin-medium bedded heterolithic clast-rich package overlain by debrite with rip-up beds and large clasts. (E) Medium-coarse sandstone bed with large mudclasts. (F) Medium-fine sandstone bed with 1 cm light bands. (G) Medium to thin sandstone beds with gravel to pebble clasts and mudstone caps. (H) Debritic sandstone-mudstone bed top with mm-1 cm shelly fragments. (I) Transition from thick dewatered and remobilised sandstone beds to mud-rich heterolithic package capped by O11 ash beds; remobilised beds are not present in the section down-dip

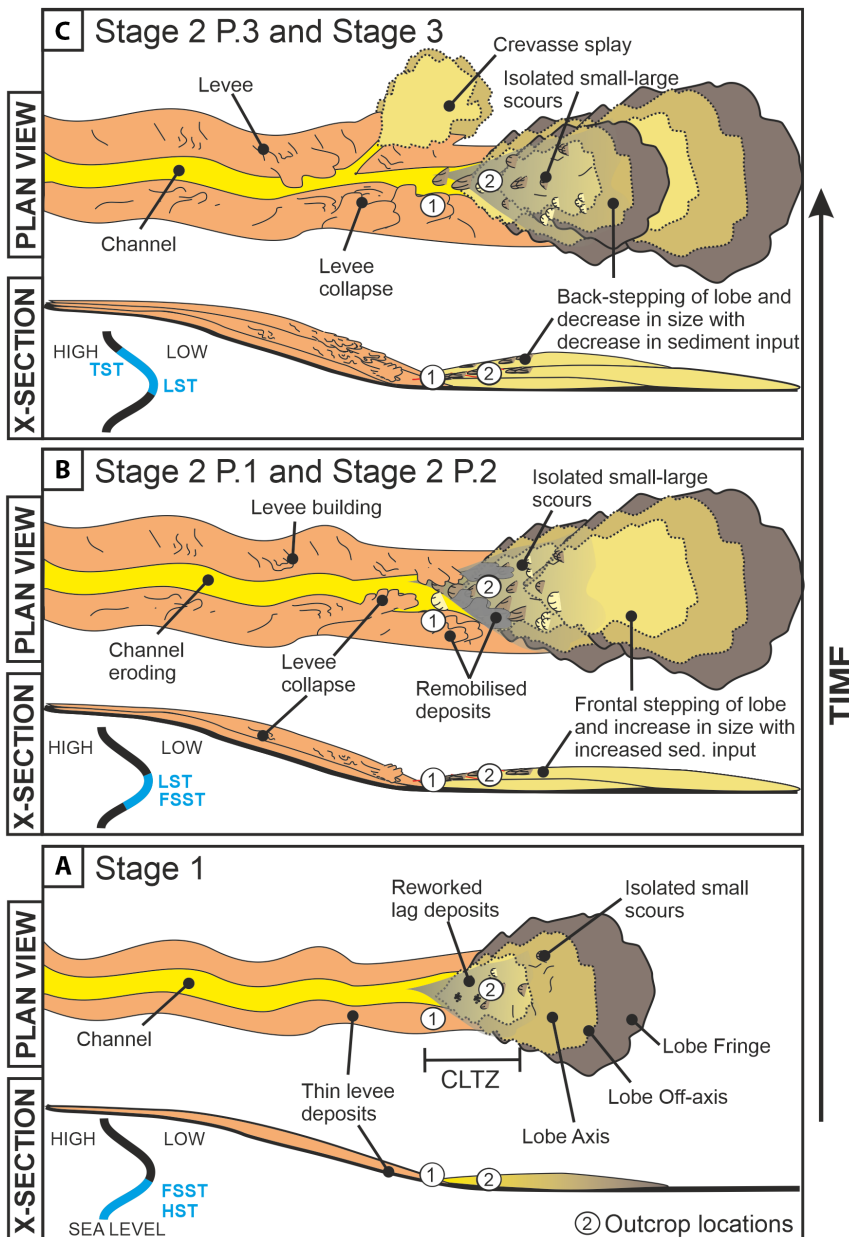


FIGURE 9 Evolution of channel-lobe transition zone. (A) Stage 1, (B) Stage 2 packages 1 and 2, and (C) Stage 2 package 3 and Stage 3, as related to relative sea-level curve, see text for further explanation and details

substrate decreases through time as a system grades to equilibrium. However, in the case of a tectonically active basin margin, the slope may be consistently above-grade (Prather et al., 2017; Figure 10) meaning large volumes of mud-rich substrate are available to be entrained throughout the duration of fan development.

It is therefore important to decipher the nature of the slope system, in order to understand the availability of mud utilised in creating hybrid beds. Although the slope gradient for the basin cannot be directly measured, Ito and Saito (2006) estimated a 3–4° mean gradient of the slope (outside of the canyon) for deposits in the Umegase and Otadai formations, based on the palaeodepth of the adjacent outer-shelf and slope deposits, which deepen to about 500 m within about an 8 km distance downslope. Based on the empirical relationship

between the submarine-fan length and lower-fan slopes from modern examples, Fukuda et al. (2015) estimated the basin-floor fan gradient as 0.3°–0.5° consistent with measurement of <1° for other basin-floor fans (Stevenson et al., 2014b). Therefore, a gradient change of 2.5–3.7° (Figure 10) is estimated at the base-of-slope. This gradient change is probably to have occurred over a short length scale due to the relatively small size of the basin, which likely varied spatially and temporally throughout the development of the system.

The Otadai Formation slope-to-basin-floor system is dominated by aggradation, as opposed to most submarine slope systems that show significant progradation (Hodgson et al., 2016), with channel-levee systems prograding over and eroding into lobe deposits. This is likely due to a high subsidence rate of 0.5–2 m/kyr (Kaizuka, 1987; Naruse,

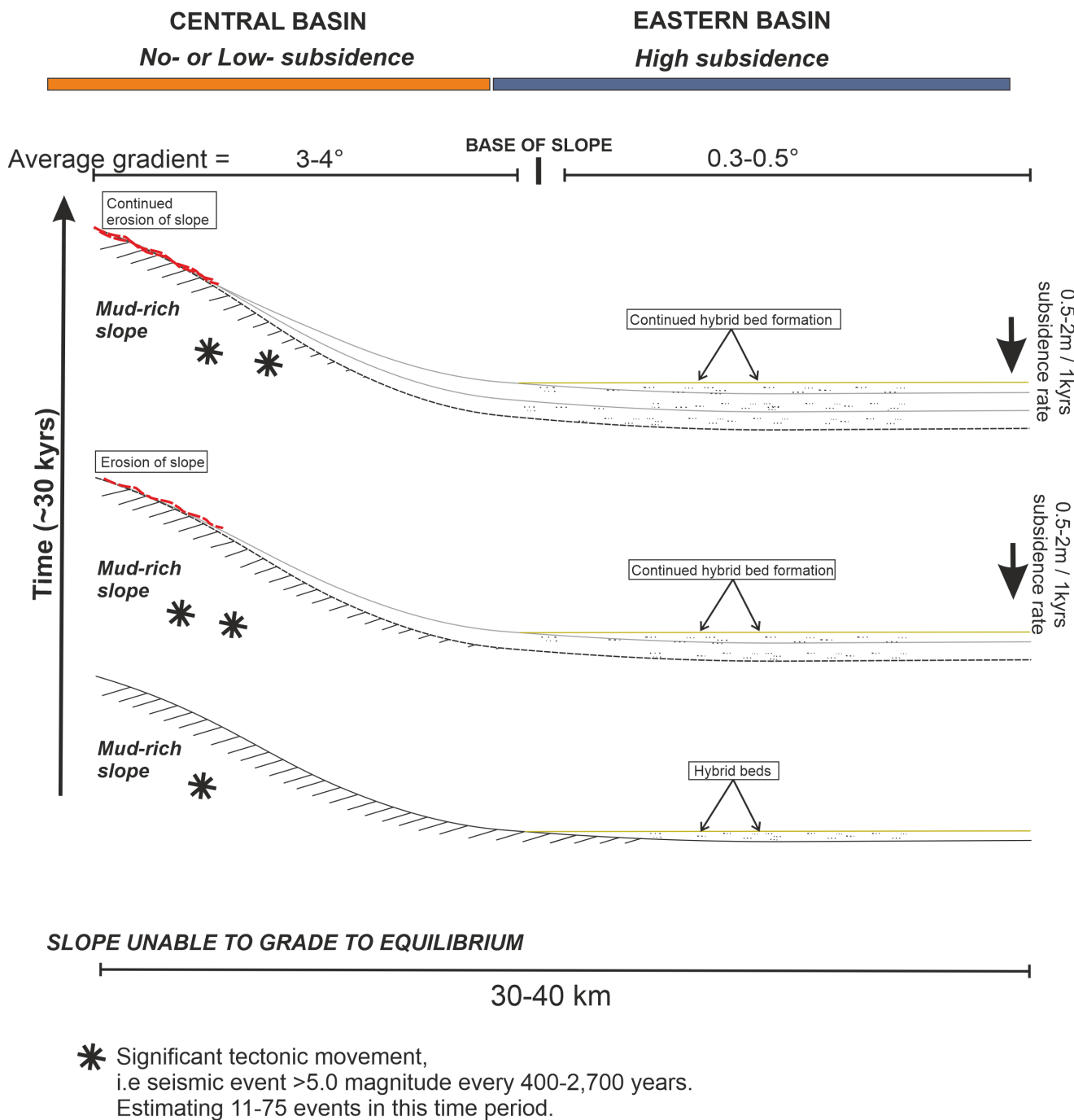


FIGURE 10 Evolution of slope to basin-floor system over deposition of outcrop section. Images from bottom to top show evolution of a slope to basin-floor profile over time. Profile cannot grade towards equilibrium due to ongoing tectonic activity and high rate of basin subsidence. The out of grade slope is eroded consistently through time, sourcing mud-rich material which is incorporated into flows allowing hybrid beds to form at the CLTZ. Earthquake periodicity from Seno et al. (1996) and Shishikura et al. (2001). Subsidence rate estimated by Naruse (1968) and Kaizuka (1987). See text for further details. Central and eastern basin terms and subsidence information from Kamiya et al. (2020)

1968), and active tectonism, which kept the system out-of-grade, as well as the Higashihigasa Formation canyon system fixing the point of input of sediment up-dip (Ito & Saito, 2006; Sato & Koike, 1957; Yamauchi et al., 1990). The out-of-grade system would consistently entrain slope sediments in order to reach equilibrium, creating a source

of erodible mud-rich substrate to drive flow transformation and the development of hybrid beds (Figure 10).

Hybrid beds are generally thought to have formed in one of several ways: (i) partial transformation of debris flow sourced from the upslope area into a forerunning turbidity current (Haughton et al., 2003); (ii) late stage

basal sand settling from a plug flow (Baas et al., 2009; Sumner et al., 2009; Talling et al., 2012); (iii) rapid deceleration of turbidity current and generation of transitional flows (Baas et al., 2011) and ultimately a debris flow (Haughton et al., 2009; Talling et al., 2004); and (iv) erosion of substrate underlying turbidity current causing bulking and damping of flow turbulence leading to (partial) transformation to a laminar flow (Amy & Talling, 2006; Fonnesu et al., 2016; Haughton et al., 2009; Mutti & Nilsen, 1981; Mutti et al., 1978; Talling et al., 2004). Kane et al. (2017) have argued that this erosion is then linked to the development of a higher-concentration lower boundary layer inhibiting transfer of turbulent kinetic energy into the upper parts of the flow, ultimately resulting in catastrophic loss of turbulence and collapse of the upper part of the flow. Overall, longitudinal change with the flow (Haughton et al., 2009), as well as vertical segregation (Baas et al., 2011) have been postulated as explanations of hybrid bed development, but these have not been previously integrated.

A more recent study by Baas et al. (2021), however, argues for longitudinal change in flows, from the head to the tail, followed by vertical segregation, as a mechanism for hybrid bed formation. Erosion is focussed preferentially at the head of the flow, causing the head to become denser, and increasing in velocity (Sequeiros et al., 2009, 2018). While the density of the head is insufficient to suspend mudclasts they travel as bedload, moving more slowly than the suspended sediment and therefore travelling back through the flow (relative to the head), and being segregated by size (Baas et al., 2021). If erosion is continuous, this frontal 'flow cell' can transform into a debris flow (Baas et al., 2021; Kane et al., 2017). Larger clasts at this point can then cut grooves (Peakall et al., 2020; Baas et al., 2021; e.g. Bed sub-types C-G, Material S1, Table 2). During flow deceleration across the CLTZ, segregation of suspended sand and mud occurs, with sand settling to form the H1 division ($d(50) = 146\text{--}235\ \mu\text{m}$, clay % = 0.91%–2.23%; Table 4), decreasing the turbulence/ increasing the cohesion in the remaining flow. The majority of the bedload will bypass with some isolated clasts being incorporated as: (i) randomly distributed clasts (e.g. Bed sub-types F and G, Material S1, Table 2); (ii) clasts near the base of the H1 division (e.g. Bed sub-types E and F, Material S1, Table 2); or (iii) concentrated along a clast horizon (e.g. Bed sub-types D, E, F G and H, Material S1, Table 2). In this study, these clast-rich horizons show a minor increase in clay percentage in the matrix ($d(50) = 132\text{--}258\ \mu\text{m}$, clay % = 2.23–4.4%, Table 4), likely due to minor disaggregation of the mudclasts. Flow deceleration at a moderate rate can increase cohesivity and result in banding, with increase in clay content present in this study ($d(50) = 65\text{--}69.9\ \mu\text{m}$, clay % = 4.65%, Table 4; e.g. Bed sub-types F and G, Material S1, Table 2; Baas et al.,

2011, 2016; Stevenson et al., 2020). A continued increase in cohesivity, aided by the disaggregation of mudclasts, resulted in the formation of the mud-rich H3 debritic division ($d(50) = 14.5\text{--}33\ \mu\text{m}$, clay % = 11.35%–20.01%, RSD = 192–375%, Table 4). This can be sub-divided into H3a and H3b, where the H3a shows some remaining minor stratification of the sand division, and the H3b is a debrite, when examined under X-ray fluorescence core scanning (Hussain et al., 2020). This may be the case for samples 1.2 and 1.3 (Table 4), in which the sorting decreases up through the H3 division (RSD = 225–295%, Table 4). Overlying H4 divisions were not identified in this study. The Baas et al. (2021) model, which combines longitudinal segregation and vertical segregation, appears to most comprehensively explain the formation of hybrid beds found in this study (Figure 10).

8.2 | Summary: why are hybrid beds abundant at this CLTZ when typically found at lobe fringes?

Overall, the increased formation and preservation of hybrid beds in this CLTZ is interpreted to be a result of: (1) The availability of erodible mud-rich substrate up-dip; (2) A persistent above grade slope (through ongoing tectonic movement/steepening due to subsidence down-dip); (3) An abrupt gradient change estimated at 2.5–3.7°; and (4) Subsiding basin-floor creating accommodation and therefore high preservation potential. The combination of erodible mud-rich substrate up-dip and a prolonged above grade slope, means that flows reaching the CLTZ will have had high mud concentrations and thus higher cohesive strength. The large gradient change then leads to moderate to rapid deceleration of flows, and a further increase in cohesive strength as the influence of turbulence decreases. This combination of high cohesive strength and moderate to rapid deceleration favours the development of hybrid event beds (rapid) and banding (moderate) (Baas et al., 2011; Stevenson et al., 2020; Sumner et al., 2009). The typical presence of hybrid beds in distal lobe locations suggests that the initial mud-content at the slope break is not normally high enough to cause the development of hybrid beds at the CLTZ. Instead, more gradual deceleration occurs across lobes, likely in combination with ingestion of fluid mud from the seafloor, leading to increasing cohesive strength and the development of hybrid beds in lobe fringes (Haughton et al., 2003, 2009; Stevenson et al., 2020; Talling et al., 2004). Finally, the combination of subsidence and high deposition rates in the present example aids the preservation of these hybrid beds, unlike CLTZs in tectonically quiescent settings where erosion across the CLTZ is far more important.

8.3 | Controls on the Otadai CLTZ development

As documented in the results, the stratigraphic evolution of Stages 1–2–3 at Location 2 shows a marked change in bed types, bed thickness, sand-to-mud ratio, amount and depth of erosion and scouring, numbers of grain-size breaks, sedimentary structures, and degree of bioturbation (Figures 6 and 7; Table 5). Overall, these changes are a record of waxing-to-waning sediment supply to the deepwater basin. The following sections discuss the factors that may have influenced the sediment supply signal and stratigraphic architecture of the measured section (spanning 30 kyr; Sugiyama & Miyata, 2015), as well as the entire Sequence 7 (spanning 50 kyr; Sugiyama & Miyata, 2015).

8.4 | Seismicity

The basin was located in a tectonically active forearc basin, formed by the subduction of the Pacific and Philippine Sea Plates under the Eurasian Plate (Ito & Masuda, 1989; Katsura, 1984). Therefore, earthquakes of magnitude >5.0 (similar to the ones impacting the study area today (e.g. EarthquakeTrack.com, ©, 2020) may have affected the basin every 400–2700 years (Seno et al., 1996; Shishikura et al., 2001; Figure 10). Thus seismic activity potentially had a strong influence on triggering flows by remobilising surficial sediments on the outer shelf and the upper slope (Kioka et al., 2019; Molenaar et al., 2019; Schwestermann et al., 2020). Furthermore, seismicity could account for the syndepositional and post-depositional bed deformation and dewatering structures (Jones & Omoto, 2000), such as those observed in BT 1, BT 2i and BT 3. Theoretically, an increase-then-decrease in seismic activity could have deposited a sedimentary succession that characterises Stage 1–2–3. However, the time encompassed in Sequence 7 (spanning 50 kyr; Sugiyama & Miyata, 2015) may be too short for such an increase-then-decrease in seismic activity to have occurred. Additionally, the major tectonic event (associated with a potential increased earthquake frequency) in the area at that time was linked with the rise of the Kujukuri-oki Anticline, which is believed to have developed after the deposition of the Otadai Formation (Furuyama et al., 2021).

8.5 | Climate and sea-level fluctuations

During the Calabrian (Early Pleistocene), glacial and interglacial cycles were oscillating at a 41 kyr frequency (Head & Gibbard, 2015), accompanied by relative

sea-level change and arid-humid climate variations. These factors combined to influence sediment supply from the hinterland drainage basins to marine sedimentary basins (Igarashi et al., 2018; Kajita et al., 2021; Nakajima et al., 2009; Sukanuma et al., 2021). The control of relative sea-level changes on the Otadai Formation has been discussed within previous studies, with Sequence 7 interpreted as reflecting an overall relative sea-level fall-then-rise cycle (Ito, 1995, 1998a, 1998b, 2008; Figure 9). This relative sea-level fall-then-rise scenario is supported by the $\delta^{18}\text{O}$ curves from benthic foraminifera (Pickering et al., 1999; Tsuji et al., 2005), which indicate an increase to decrease to increase in $\delta^{18}\text{O}$ values between ash beds O16 and O11. This supports the hypothesis that relative sea-level change was (one of) the main overall driver(s) for much of the variability noted between Stages 1–2–3 at Location 2 (Figure 9). Indeed, Stages 1 and 2 recorded an increased sediment transport to the base-of-slope associated with high-energy flows, reflecting deposition that occurred during a relative sea-level fall and lowstand (Figure 9A,B). It is possible that the rapid relative sea-level fluctuations during the Calabrian could have led to local instabilities through periods of reduced sediment input to the shelf during the transition to glacial and more arid periods. These slope instabilities, in turn, generated surge-type turbidity currents (Nakajima et al., 2009). The thinning- and fining-upward trends that characterise Stage 3 supports deposition during a subsequent transgressive phase (Figure 9C), while the overlying mud-dominated interval of Sequence 7, which caps the measured section (e.g. Figure 2C; Ito, 1998a), was deposited during a relative sea-level highstand.

If the overall Sequence 7 recorded one 41 kyr obliquity-driven interglacial-to-glacial-to-interglacial cycle (Igarashi et al., 2018; Kajita et al., 2021; Nakajima et al., 2009; Sukanuma et al., 2021), then development of Package 1, 2 and 3 in stage 2 could reflect shorter-lived cycles. For example (half-?) precession-driven cycles, which seem to have gradually increased in intensity during the '41 kyr Pleistocene world' (Liautaud et al., 2020 and references therein).

In addition to these glacioeustatic sea-level variations, there is evidence of significant climate shifts occurring during the deposition of the upper Otadai Formation. Momohara (1994) suggested that the floral changes, which occurred at 1.1 Ma in central Japan, indicate that climate fluctuations became frequent and occurred at less than 100 kyr intervals. Igarashi et al. (2018) showed that significant orbital-scale cyclical variations in both temperature and precipitation occurred in the hinterland of the Kazusa Basin during deposition of the Otadai Formation. These climate variations were derived from palynological data and interpreted to reflect glacial and interglacial

cycles driven by 41 kyr orbital forcing (Igarashi et al., 2018), associated with changes in regional ocean circulation (Suganuma et al., 2021). Moreover, interglacial periods in the Kazusa Basin were associated with increased intensity and a northwards extension of the Kuroshio Current in comparison to glacial periods, circulating more warm water masses from the Western Pacific Warm Pool to the study area (Ito, 1992; Kajita et al., 2021; Takao et al., 2020). Sea surface temperatures in the Kazusa Basin, derived from planktonic foraminifera, have varied from 22.5–24.8°C during interglacial periods (MIS-33, 31, 29) to 19.9–21.9°C during glacial periods (MIS-32, 30; Kajita et al., 2021). Increased sea surface temperatures during interglacial periods might have been associated with an increased tropical cyclone frequency and intensity (Zhang et al., 2020), as well as potentially enhanced monsoonal activity (Liu et al., 2020). Increased monsoonal activity and tropical cyclone frequency and intensity during interglacial periods would have led to accentuated coastal erosion by waves (Nishida et al., 2020), as well as increased precipitation and weathering in the hinterland of the Kazusa Basin, resulting in higher river discharge and increased sediment delivery to the shelf (Joussain et al., 2016; Rice et al., 2020).

The potential impact of these sediment supply variations on the deepwater system would have been out-of-phase with the influence of the recorded glacioeustasy. The coarsest and thickest strata of Stage 2 could have been deposited during a highstand period associated with a climate optimum and an increased sediment input to the shelf. Sediment storage is limited on narrow and steep shelves during relative sea-level highstand on active continental margins (Covault & Graham, 2010; Covault et al., 2007; Harris & Wiberg, 2002), such as the one that prevailed when the Otadai Formation was being deposited. This shelf geometry restricts sediment storage capacity, particularly when sediment supply increases, and sand-rich flows can still traverse the shelf and slope (Blum & Hattier-Womack, 2009; Bouma, 2000; Nakajima et al., 2009; Postma et al., 1993; Prins et al., 2000; Weltje & de Boer, 1993). It is possible that the canyon feeding the deepwater system of the Otadai Formation was disconnected from the shoreline during relative sea-level highstands, which would have prevented sediments from being transported further down the canyon. If the canyon had been connected to the shoreline, the deepwater system of the Otadai Formation would have been much more active during periods of relative sea-level highstand (Covault & Graham, 2010; Covault et al., 2007; Fisher et al., 2021; Sweet & Blum, 2016). Additionally, during interglacial periods, a strengthened Kuroshio Current (Ito, 1992; Kajita et al., 2021; Nishida et al., 2020; Takao et al., 2020) would have helped the shelf redistribution of sediment brought

there by an increase in coastal wave erosion (Nishida et al., 2020; Nishida & Ikehara, 2013) associated with an enhanced tropical cyclone frequency and intensity (Zhang et al., 2020). This potentially prevented most sediment transfer from the shelf down the slope to the Otadai deepwater system.

The 41 kyr-duration, obliquity-driven glacial-interglacial cycles and associated relative sea-level change were the dominant factors influencing the development of Sequence 7 and these CLTZ deposits, and by extension, the entire Otadai Formation, in agreement with previous authors (Ito, 1995, 1998a, 2008; Pickering et al., 1999; Tsuji et al., 2005). The signal of increased sediment supply to the shelf during humid interglacial periods was likely subdued by the absence of a conduit connected to the shoreline, and the presence of the Kuroshio Current strong enough to redistribute most of the sediment along the narrow shelf. In this context, intrinsic controls such as lobe stacking (Brooks et al., 2018b; Grundvåg et al., 2014; Hodgson et al., 2006, 2016; Mutti & Sonnino, 1981; Prélat et al., 2009, 2010; Pyrcz et al., 2005), variations of flow efficiency associated with change in upstream channel dimension (Fildani et al., 2013), or variations of channel sinuosity and the associated filtering effect (Amos et al., 2010), were restricted to modulating the development of the Otadai Formation CLTZ.

8.6 | Comparing CLTZs in tectonically active and tectonically quiescent margins

This study compares the diagnostic criteria, dimensions and evolution of CLTZs in active margins and tectonically quiescent basins in order to distinguish the key differences and similarities (Figure 11; Table 6). The example presented in this study appears to be controlled primarily by extrinsic factors (i.e. sea-level fluctuation and tectonics). These variable factors mean that the slope system most likely cannot reach equilibrium (Prather, 2000, 2003) throughout the CLTZ development. In active margins, due to ongoing erosion on the slope, there is a sustained availability of mud-rich substrate leading to enhanced hybrid bed development (Figures 10 and 11C). The debritic mud-rich H3 divisions are characterised by an average grain size of fine to coarse silt ($d(50) = 14.5\text{--}33\ \mu\text{m}$, Table 4), a high clay percentage (clay % = 11.35%–20.01%, Table 4) and a poor sorting (RSD = 192%–375%, Table 4). The diversity of hybrid bed types, including banded divisions, indicates variations in flow deceleration rates, due to differences in grain size and velocity of flows, and/or the gradient and magnitude of slope breaks. Specifically, throughout the deposition of the Otadai Formation (3 to 1 Ma), the eastern area of the Kazusa Basin, at and down-dip of the study

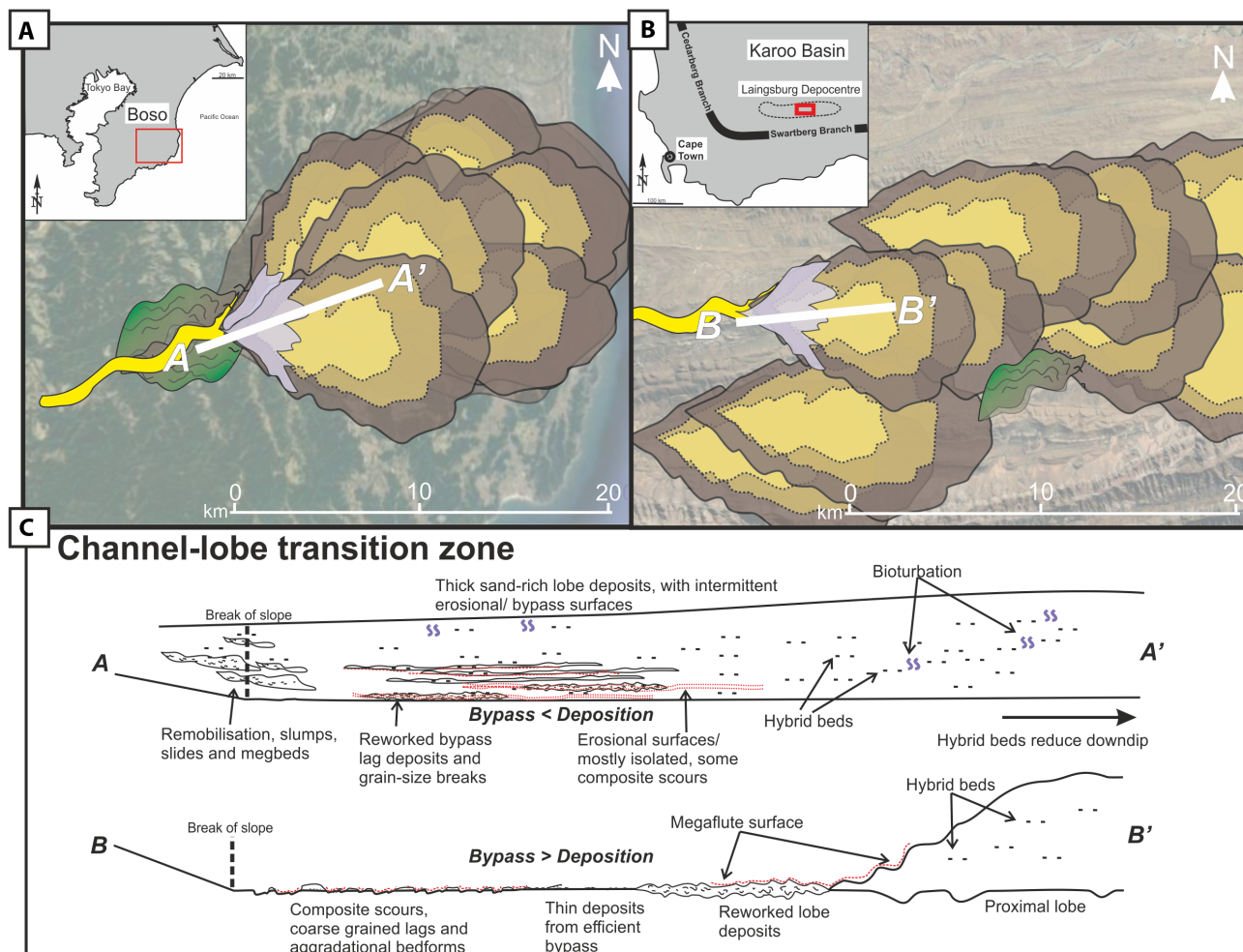


FIGURE 11 Comparison of CLTZ size, dimensions and architecture between this example (A) and an example from Unit E of the Fort Brown Formation, Karoo Basin, South Africa (information from Brooks et al., 2018a, 2018b) (B and C) Shows the key characteristics in a down-dip transect through both channel lobe transition zones; see text for details. The Otadai example (A) is more fixed in location whereas the Unit E CLTZ (B) is more dynamic, expanding/contracting or shifting spatially through time (Brooks et al., 2018a)

area, subsided more than in the western part of the basin, which started up-lifting after 1 Ma (Kamiya et al., 2020). This basinward tilting pattern may have helped to sustain erosion of the slope in the western area (immediately up-dip of the study location) as the slope worked towards equilibrium, as well as the continued entrenchment of the Higashihigasa canyon (Ito & Saito, 2006; Sato & Koike, 1957; Yamauchi et al., 1990). This suggests that the locus of subsidence along narrow active margins is spatially constrained and remains more fixed in a dip-direction through time than in tectonically quiescent basins, where the locus of subsidence can be broader or migrate along the dip transect of wide passive margins. As a result, the high rates of subsidence on the basin-floor, the spatially fixed locus of subsidence and sediment input created a thick, aggradational system dominated by depositional processes (Figure 10). Periods of sediment bypass occurred, as evidenced by lags and grain-size breaks and scour-fills, but these are dispersed throughout the stratigraphy, and

rarely coalesce or form composite surfaces due to this high sedimentation rate (Figure 11C). In contrast, Mansor and Amir Hassan (2021) explain the high number of hybrid beds in an interpreted exhumed CLTZ in a tectonically active basin (the Oligocene-Miocene Tajau Sandstone Member Sabah, Malaysia) by intrinsic controls. In this case, repeated flow transformation of turbidity currents is interpreted to be driven by flow deflection and deceleration against a confining counter slope close to a sediment entry point in a narrow basin.

In comparison, examples of well-exposed CLTZs in tectonically quiescent basins, such as Unit E3 of the Permian Fort Brown Formation in the Karoo Basin (Brooks et al., 2018a; van der Merwe et al., 2014), are characterised by more bypass and erosion (Figure 11B,C), a thinner stratigraphic expression (metres to a few tens of metres) and more composite scour surfaces (Figure 11C, Table 6). Hybrid beds in the Fort Brown Formation example are present in the proximal lobe area, and are

TABLE 6 Key basinal factors and CLTZ characteristics in the active Kazusa Basin during deposition of the Otadai Formation, and Sub-unit E3 of the Permian Fort Brown Formation of the Karoo Basin, South Africa

	Kazusa	Karoo
Basin		
Sediment input	Fixed location (Canyon) (Ito et al., 2014)	Several locations
Slope conduit	Canyon-channel system (Ito et al., 2014)	Entrenched channels (Brooks et al., 2018a; van der Merwe et al., 2014)
Sediment source distance and provenance	Siliciclastics sourced central Japan? Local volcanic source for minor volcanoclastic input	Long distance, Antarctica igneous massif (McKay et al., 2016)
Duration of formation (1 sea-level cycle approx.)	0.21 My (Otadai Formation) (50,000 years Cycle 7; Ito & Katsura, 1992; Ito, 1998a, 2008; Takano et al., 2004).	6 My (Collingham, Vishkuil, Laingsberg and Fort Brown Formations; Belica et al., 2017; Lanci et al., 2013; McKay et al., 2015). 1.2 My(?)* per formation. Fort Brown Formation (Unit C, D, E, F, G), 0.24 My(?)* per Unit. Unit E1, E2 and E3 (80,000 yrs Unit E3)* *Very rough estimate assuming linear deposition
Basin evolution	Active tectonics—Creating accommodation throughout infill (Ito, 1992)	No active tectonics—Accommodation through sag of basin, differential subsidence and compaction (Brooks et al., 2018a)
Climate	Similar to today, glacial/interglacial at altitude (Ito & Katsura, 1992; Pickering et al., 1999)	Post glacial—cool climate (Smith et al., 1993)
Grain size	Clay-Boulder (Ito et al., 2014)	Silt-fine sand (Brooks et al., 2018a)
CLTZ		
Stratigraphy	Sand-attached (<i>sensu</i> Mutti, 1985), volume of rock	Sand-detached (<i>sensu</i> Mutti, 1985), traceable surface (Brooks et al., 2018b; van der Merwe et al., 2014)
Scours	Yes- Depth: mm- several m's Generally isolated	Yes- Depth: mm to several m's Isolated and composite (Brooks et al., 2018a)
Sediment waves	No	Remnant- Fine sandstone, Metre scale Spaced stratification, climbing ripples + sheared climbing ripples (Brooks et al., 2018a)
Grain-size breaks	Yes	Not recognisable at outcrop (Brooks et al., 2018a)
Lags	Few with large angular clasts	Yes, numerous, mix of fine (+lower medium) sand and mudclasts (Brooks et al., 2018a)
Hybrid beds	Yes- Numerous, range of bed types	Yes, only in proximal lobe, sand-rich, 1 bed type (Brooks et al., 2018a)
Abandonment	Gradual- Switch to off-axis lobe	Abrupt- Sudden avulsion or shut off of sediment supply (Brooks et al., 2018a)
Palaeogeographic context	Overbank deposits up-dip 4.5 km Lobe deposits down-dip 4.7 km Max CLTZ length 9.2 km Width of zone >700 m (Ito, 2008)	Can walk out up-dip levee and down-dip lobe deposits Max CLTZ length 6 km Width <12 km (Brooks et al., 2018a)

sand-rich (by observation, no grain-size measurements available), with no banding or other diversity in bed types. The availability of mud-rich substrate was likely confined to the interval of erosion and bypass of the CLTZ immediately up-dip (Brooks et al., 2018a), so that hybrid beds only formed immediately down-dip (within 1–2 km), and are not present any further down the system (Brooks et al., 2018a; van der Merwe et al., 2014).

Moreover, this CLTZ migrated, recording phases of contraction/expansion. It was associated with shifting of up-dip channel/levee systems and down-dip lobe complexes (Brooks et al., 2018a), which contrasts with the more fixed position of the Otadai CLTZ. Despite the differences, the two CLTZs are likely roughly comparable in size (few kilometres in length and width, Figure 11, Table 6), in contrast to examples from the modern that

can be 30–120 km in length (Kenyon et al., 1995; Kenyon & Millington, 1995; Morris et al., 1998; Palanques et al., 1995; Wynn et al., 2002).

The abundance and diversity of hybrid beds noted in the Otadai Formation CLTZ is rare, but not unique. A recently published example from the Aberystwyth Grits Group (Baas et al., 2021), within the Silurian deposits of the back-arc Welsh Basin (Kokelaar et al., 1984), also documents a significant range of hybrid beds within a CLTZ (Baas et al., 2021). Due to outcrop constraints, the exact basin configuration is unknown in this Welsh Basin example, so it is not possible to compare the up-dip slope condition to the slope of the Otadai Formation system. This 1.6 km long down-dip section records a transition from channel/levee deposits, through a CLTZ, to lobe axis and off-axis environments (Baas et al., 2021). It is noted that the CLTZ contains thicker beds with less common erosional scours when compared to the CLTZ of Unit E in the Karoo Basin, and that the hybrid bed component may indicate deposition concentrated towards the lobe rather than the channel (within the CLTZ). Overall, the example described by Baas et al. (2021) is likely smaller in spatial extent but is largely unconstrained (roughly an order of magnitude thinner; Baas et al., 2021) and has a thinner stratigraphic expression than the CLTZ of the Otadai Formation system. However, it does demonstrate that an abundance of hybrid beds is not unique to the Otadai Formation CLTZ. This therefore emphasises that abundant hybrid beds in outcrop or core are not necessarily indicative of lobe fringe environments (Spychala et al., 2017a, 2017b). Instead, hybrid beds are indicative of an availability of erodible mud-rich substrate up-dip of the deposits, associated with conditions that allow both longitudinal and vertical segregation within the flow (Baas et al., 2021), independent of the environment and tectonic setting. Indeed, any basin margin with basinward tilting and a mud-rich substrate are primed to generate hybrid beds. This could include tectonically quiescent post-rift settings where canyon positions are fixed (Jackson et al., 2021).

9 | CONCLUSIONS

This study documents the evolution of a CLTZ preserved in the Pleistocene Otadai Formation, cropping out on the Boso Peninsula, Chiba, Japan. This deepwater succession spanning 50 kyr recorded a full relative sea-level fall-then-rise cycle, which is constrained by the presence of two regionally correlated ash beds. Based on variations in grain size, bed thickness, degree of amalgamation, stacking pattern and sedimentary architecture, the succession was subdivided into three stages (Stages 1–3). These stages show an increase followed by a decrease in: bed thickness; sand content; and erosional/ bypass indicators.

Observations of the abundant and diverse hybrid beds noted in the Otadai Formation CLTZ most closely fit with models of hybrid bed formation that integrate longitudinal segregation from the head to the tail of the flow, and vertical stratification from base to top. The presence of hybrid beds throughout fan development (and not just in frontal lobes) was likely a factor of a continuously above grade slope, unable to reach equilibrium due to high subsidence rates and ongoing tectonic activity. These factors will have accentuated erosion on the slope, providing sufficient mud-rich sediment to drive flow transformation, and form hybrid beds at the CLTZ.

Despite modulation from intrinsic controls, the overall coarsening then fining-upwards trend of this 50 kyr succession is thought to predominantly reflect an overall obliquity-driven relative sea-level fall-then-rise cycle, associated with a change from interglacial through glacial to interglacial climate conditions. During interglacial periods, the combination of a conduit disconnected from the shoreline, and a Kuroshio Current strong enough to redistribute shelf sediment freshly brought by an enhanced coastal wave erosion, likely hindered sediment transfer down-dip to the Otadai Formation deepwater system.

Compared to tectonically quiescent basin examples, CLTZs developing along active margins, such as that examined in this study consist of: (i) significantly thicker stratigraphy and more isolated and smaller scours, likely due to high sedimentation and subsidence rates; (ii) fewer bypass lags, which are only present at the base of the section and are significantly reworked; (iii) more common grain-size breaks, likely recognised due to wider grain-size range; and (iv) a higher proportion and diversity of hybrid beds, due to high availability of mud-rich erodible substrate. Additionally, CLTZs along active margins are characterised by a fixed and aggradational position at the base-of-slope, in contrast with the shifting, contracting and expanding behaviour of their counterparts in tectonically quiescent basins. Consequently, CLTZs along active margins are less interstratified with sediments from adjacent palaeoenvironments, compared to dynamic CLTZs in tectonically quiescent systems. This fixed and aggradational behaviour of CLTZs along active margins is thought to reflect a subsidence-to-sedimentation rate ratio, which prevented the slope up-dip of the CLTZ from prograding and changing its geometry, and certainly not by as much as it would in tectonically quiescent basins. Intrinsic controls, therefore, are more influential on the nature and the dynamic of the flows, and the resulting architecture of CLTZs, in tectonically quiescent basins. This suggests that there is a much greater diversity in CLTZ deposits than has previously been recognised, but also suggests that these are broadly predictable based on the relative degree of tectonic activity, the amount of accommodation and the availability of mud as an input to the system.

ACKNOWLEDGEMENTS

The authors would like to thank the Japan Society for Promotion of Science for funding this study, through the JSPS Postdoctoral Fellowships for Research in Japan Short-Term Program. They also thank Amer Shehata, Miyazawa Yoshihiro, Junichi Takahashi and Alexis Demorsy for assistance in the field. Finally, they thank Dr Thomas Dodd, an anonymous reviewer and the associate editor for helpful comments on the manuscript.

CONFLICT OF INTEREST

There is no conflict of interest in the preparation or publication of this work.

ORCID

Hannah L. Brooks  <https://orcid.org/0000-0002-3772-7372>
 Valentin Zuchuat  <https://orcid.org/0000-0002-2029-6422>
 David M. Hodgson  <https://orcid.org/0000-0003-3711-635X>

REFERENCES

- Allen, J.R.L. (1970) A quantitative model of climbing ripples and their cross-laminated deposits. *Sedimentology*, *14*, 5–26. <https://doi.org/10.1111/j.1365-3091.1970.tb00179.x>
- Allen, J.R.L. (1983) Gravel overpassing on humpback bars supplied with mixed sediment: examples from the Lower Old Red Sandstone, southern Britain. *Sedimentology*, *30*, 285–294.
- Amos, K.J., Peakall, J., Bradbury, P.W., Roberts, M., Keevil, G. & Gupta, S. (2010) The influence of bend amplitude and planform morphology on flow and sedimentation in submarine channels. *Marine and Petroleum Geology*, *27*, 1431–1447.
- Amy, L.A. & Talling, P.J. (2006) Anatomy of turbidites and linked debrites based on long distance (120× 30 km) bed correlation, Marnoso Arenacea Formation, Northern Apennines, Italy. *Sedimentology*, *53*(1), 161–212.
- Baas, J.H., Best, J.L. & Peakall, J. (2011) Depositional processes, bedform development and hybrid flows in rapidly decelerated cohesive (mud-sand) sediment flows. *Sedimentology*, *58*, 1953–1987.
- Baas, J.H., Best, J.L. & Peakall, J. (2016) Predicting bedforms and primary current stratification in cohesive mixtures of mud and sand. *Journal of the Geological Society*, *173*, 12–45.
- Baas, J.H., Best, J.L., Peakall, J. & Wang, M. (2009) A phase diagram for turbulent, transitional, and laminar clay suspension flows. *Journal of Sedimentary Research*, *79*, 162–183.
- Baas, J.H., Tracey, N.D. & Peakall, J. (2021) Sole marks reveal deep-marine depositional process and environment: implications for flow transformation and hybrid event bed models. *Journal of Sedimentary Research*, *91*, 986–1009.
- Baba, K. (1990) Molluscan Fossil Assemblages of the Kazusa Group. South Kwanto, Central Japan (in Japanese). Tokyo: Keiyo Yochisha, p. 445.
- Baker, M.L. & Baas, J.H. (2020) Mixed sand-mud bedforms produced by transient turbulent flows in the fringe of submarine fans: indicators of flow transformation. *Sedimentology*, *67*, 2645–2671.
- Belica, M.E., Tohver, E., Pisarevsky, S.A., Jourdan, F., Denyszyn, S. & George, A.D. (2017) Middle Permian paleomagnetism of the Sydney Basin, Eastern Gondwana: testing Pangea models and the timing of the end of the Kiaman Reverse Superchron. *Tectonophysics*, *699*, 178–198.
- Bell, D., Kane, I.A., Pontén, A.S., Flint, S.S., Hodgson, D.M. & Barrett, B.J. (2018) Spatial variability in depositional reservoir quality of deep-water channel-fill and lobe deposits. *Marine and Petroleum Geology*, *98*, 97–115.
- Blum, M.D. & Hattier-Womack, J. (2009) Climate change, sea-level change, and fluvial sediment supply to deepwater depositional systems. In: Kneller, B., Martinsen, O.J. & McCaffrey, B. (Eds.) *External controls on deep water depositional systems. SEPM Special Publication*, *92*, pp. 15–39.
- Bouma, A.H. (2000) Coarse-grained and fine-grained turbidite systems as end member models: applicability and dangers. *Marine and Petroleum Geology*, *17*, 137–143.
- Brooks, H.L., Hodgson, D.M., Brunt, R.L., Peakall, J., Hofstra, M. & Flint, S.S. (2018a) Deepwater channel-lobe transition zone dynamics: processes and depositional architecture, an example from the Karoo Basin, South Africa. *Geological Society of America Bulletin*, *130*, 1723–1746. <https://doi.org/10.1130/B31714.1>
- Brooks, H.L., Hodgson, D.M., Brunt, R.L., Peakall, J., Poyatos-Moré, M. & Flint, S.S. (2018b) Disconnected submarine lobes as a record of stepped slope evolution over multiple sea-level cycles. *Geosphere*, *14*, 1753–1779.
- Carvajal, C., Paull, C.K., Caress, D.W., Fildani, A., Lundsten, E., Anderson, K., Maier, K.L., McGann, M., Gwiadzda, R. & Herguera, J.C. (2017) Unraveling the channel-lobe transition zone with high-resolution AUV bathymetry: Navy Fan, offshore Baja California, Mexico. *Journal of Sedimentary Research*, *87*, 1049–1059.
- Covault, J.A. & Graham, S.A. (2010) Submarine fans at all sea-level stands: tectono-morphologic and climatic controls on terrigenous sediment delivery to the deep sea. *Geology*, *38*, 939–942.
- Covault, J.A., Normark, W.R., Romans, B.W. & Graham, S.A. (2007) Highstand fans in the California borderland: the overlooked deep-water depositional systems. *Geology*, *35*, 783–786.
- Cunha, R.S., Tinterri, R. & Muzzi Magalhaes, P. (2017) Annot Sandstone in the Peira Cava basin: an example of an asymmetric facies distribution in a confined turbidite system (SE France). *Marine and Petroleum Geology*, *87*, 60–79.
- Droz, L., Jégou, I., Gillet, H., Dennielou, B., Bez, M., Canals, M., Amblas, D., Lastras, G. & Rabineau, M. (2020) On the termination of deep-sea fan channels: examples from the Rhône Fan (Gulf of Lion, Western Mediterranean Sea). *Geomorphology*, *369*, 107368.
- Earthquaketrack.com©. 2020 Earthquake Track. Visited 12.08.2020. <https://earthquaketrack.com/p/japan/chiba/recent>
- Fildani, A., Hubbard, S.M., Covault, J.A., Maier, K.L., Romans, B.W., Traer, M. & Rowland, J.C. (2013) Erosion at inception of deep-sea channels. *Marine and Petroleum Geology*, *41*, 48–61.
- Fisher, W.L., Galloway, W.E., Steel, R.J., Olariu, C., Kerans, C. & Mohrig, D. (2021) Deep-water depositional systems supplied by shelf-incising submarine canyons: recognition and significance in the geologic record. *Earth-Science Reviews*, *214*, 103531.
- Fonnesu, M., Felletti, F., Haughton, P.D., Patacci, M. & McCaffrey, W.D. (2018) Hybrid event bed character and distribution linked to turbidite system sub-environments: the North Apennine Gottero Sandstone (north-west Italy). *Sedimentology*, *65*, 151–190.

- Fonnesu, M., Patacci, M., Haughton, P.D., Felletti, F. & McCaffrey, W.D. (2016) Hybrid event beds generated by local substrate delamination on a confined-basin floor. *Journal of Sedimentary Research*, *86*, 929–943.
- Friedman, G.M. (1962) On sorting, sorting coefficients, and the lognormality of the grain-size distribution of sandstones. *The Journal of Geology*, *70*, 737–753.
- Fukuda, K., Suzuki, M. & Ito, M. (2015) The origin and internal structures of submarine-slide deposits in a lower Pleistocene outer-fan succession in the Kazusa forearc basin on the Boso Peninsula of Japan. *Sedimentary Geology*, *321*, 70–85.
- Furuyama, S., Sato, T., Arai, K. & Ozaki, M. (2021). Tectonic evolution in the early to Middle Pleistocene off the east coast of the Boso Peninsula, Japan. In: Asch, K., Kitazato, H. & Vallius, H. (Eds.) *From continental shelf to slope: mapping the oceanic realm*. Geological Society, London, Special Publications, 505. doi: <https://doi.org/10.1144/SP505-2019-116>
- Galloway, W.E. (1998) Siliciclastic slope and base-of-slope depositional systems: component facies, stratigraphic architecture, and classification. *AAPG Bulletin*, *82*, 569–595.
- Gardner, M.H., Borer, J.A., Melick, J.J., Mavilla, N., Dechesne, M. & Wagerle, R.N. (2003) Stratigraphic process-response model for submarine channels and related features from studies of Permian Brushy Canyon outcrops, West Texas. *Marine and Petroleum Geology*, *20*, 757–787. <https://doi.org/10.1016/j.marpetgeo.2003.07.004>
- Gladstone, C., McClelland, H.L., Woodcock, N.H., Pritchard, D. & Hunt, J.E. (2018) The formation of convolute lamination in mud-rich turbidites. *Sedimentology*, *65*, 1800–1825.
- Gladstone, C. & Sparks, R.S.J. (2002) The significance of grain-size breaks in turbidites and pyroclastic density current deposits. *Journal of Sedimentary Research*, *72*, 182–191.
- Grundvåg, S.A., Johannessen, E.P., Helland-Hansen, W. & Plink-Björklund, P. (2014) Depositional architecture and evolution of progradationally stacked lobe complexes in the Eocene Central Basin of Spitsbergen. *Sedimentology*, *61*, 535–569.
- Harris, C.K. & Wiberg, P. (2002) Across-shelf sediment transport: interactions between suspended sediment and bed sediment. *Journal of Geophysical Research: Oceans*, *107*, C13008.
- Haughton, P.D., Barker, S.P. & McCaffrey, W.D. (2003) ‘Linked’ debrites in sand-rich turbidite systems—origin and significance. *Sedimentology*, *50*, 459–482.
- Haughton, P., Davis, C., McCaffrey, W. & Barker, S. (2009) Hybrid sediment gravity flow deposits—classification, origin and significance. *Marine and Petroleum Geology*, *26*, 1900–1918.
- Head, M.J. & Gibbard, P.L. (2015) Early-Middle Pleistocene transitions: linking terrestrial and marine realms. *Quaternary International*, *389*, 7–46.
- Hirayama, J. & Nakajima, T. (1977) Analytical study of turbidites, Otadai Formation, Boso Peninsula, Japan. *Sedimentology*, *24*, 747–779.
- Hodgson, D.M. (2009) Origin and distribution of bipartite beds in sand-rich submarine fans: constraints from the Tanqua depocentre, Karoo Basin, South Africa. *Marine and Petroleum Geology*, *26*, 1940–1956. <https://doi.org/10.1016/j.marpetgeo.2009.02.011>
- Hodgson, D.M., Flint, S.S., Hodgetts, D., Drinkwater, N.J., Johannessen, E.P. & Luthi, S.M. (2006) Stratigraphic evolution of fine-grained submarine fan systems, Tanqua depocenter, Karoo Basin, South Africa. *Journal of Sedimentary Research*, *76*, 20–40.
- Hodgson, D.M., Kane, I.A., Flint, S.S., Brunt, R.L. & Ortiz-Karpp, A. (2016) Time-transgressive confinement on the slope and the progradation of basin-floor fans: implications for the sequence stratigraphy of deep-water deposits. *Journal of Sedimentary Research*, *86*, 73–86.
- Hofstra, M., Hodgson, D.M., Peakall, J. & Flint, S.S. (2015) Giant scour-fills in ancient channel-lobe transition zones: formative processes and depositional architecture. *Sedimentary Geology*, *329*, 98–114. <https://doi.org/10.1016/j.sedgeo.2015.09.004>
- Hofstra, M., Peakall, J., Hodgson, D.M. & Stevenson, C.J. (2018) Architecture and morphodynamics of subcritical sediment waves in an ancient channel-lobe transition zone. *Sedimentology*, *65*, 2339–2367.
- Horikawa, K. & Ito, M. (2004) Long-term ENSO-like events represented in the Middle Pleistocene shelf successions, Boso Peninsula, Japan. *Palaeogeography, Palaeoclimatology, Palaeoecology*, *203*, 239–251.
- Hussain, A., Haughton, P.D., Shannon, P.M., Turner, J.N., Pierce, C.S., Obradors-Latre, A., Barker, S.P. & Martinsen, O.J. (2020) High-resolution X-ray fluorescence profiling of hybrid event beds: implications for sediment gravity flow behaviour and deposit structure. *Sedimentology*, *67*, 2850–2882.
- Igarashi, Y., Irino, T., Sawada, K., Song, L. & Furota, S. (2018) Fluctuations in the East Asian monsoon recorded by pollen assemblages in sediments from the Japan Sea off the south-western coast of Hokkaido, Japan, from 4.3 Ma to the present. *Global and Planetary Change*, *163*, 1–9.
- Inami, K. (1981) Mechanical properties of mudstone in the Boso Peninsula. *Journal of the Japanese Association for Petroleum Technology*, *46*, 1–10 (in Japanese).
- Ishiwada, Y., Mitsunashi, T., Shinada, Y. & Makino, T. (1971) Geological maps of the oil and gas field of Japan; 10, Mobara. Geological Survey of Japan Map, scale 1:50,000.
- Ito, M. (1992) High-frequency depositional sequences of the upper part of the Kazusa Group, a middle Pleistocene forearc basin fill in Boso Peninsula, Japan. *Sedimentary Geology*, *76*, 155–175.
- Ito, M. (1994) Compositional variation in depositional sequences of the upper part of the Kazusa Group, a middle Pleistocene forearc basin fill in the Boso Peninsula, Japan. *Sedimentary Geology*, *88*, 219–230.
- Ito, M. (1995) Volcanic ash layers facilitate high-resolution sequence stratigraphy at convergent plate margins: an example from the Plio-Pleistocene forearc basin fill in the Boso Peninsula, Japan. *Sedimentary Geology*, *95*, 187–206.
- Ito, M. (1996) Sandy contourites of the lower Kazusa Group in the Boso Peninsula, Japan; Kuroshio-current-influenced deep-sea sedimentation in a Plio-Pleistocene forearc basin. *Journal of Sedimentary Research*, *66*, 587–598.
- Ito, M. (1998a) Submarine fan sequences of the lower Kazusa Group, a Plio-Pleistocene forearc basin fill in the Boso Peninsula, Japan. *Sedimentary Geology*, *122*, 69–93.
- Ito, M. (1998b) Contemporaneity of component units of the lowstand systems tract: an example from the Pleistocene Kazusa forearc basin, Boso Peninsula, Japan. *Geology*, *26*(10), 939–942.
- Ito, M. (2008) Downfan transformation from turbidity currents to debris flows at a channel-to-lobe transitional zone: the lower Pleistocene Otadai Formation, Boso Peninsula, Japan. *Journal of Sedimentary Research*, *78*, 668–682.

- Ito, M., Ishikawa, K. & Nishida, N. (2014) Distinctive erosional and depositional structures formed at a canyon mouth: a lower Pleistocene deep-water succession in the Kazusa forearc basin on the Boso Peninsula, Japan. *Sedimentology*, *61*, 2042–2062.
- Ito, M., Ishimoto, S., Ito, K. & Kotake, N. (2016) Geometry and lithofacies of coarse-grained injectites and extrudites in a late Pliocene trench-slope basin on the southern Boso Peninsula, Japan. *Sedimentary Geology*, *344*, 336–349.
- Ito, M. & Katsura, Y. (1992) Inferred glacio-eustatic control for high-frequency depositional sequences of the Plio-Pleistocene Kazusa Group, a forearc basin fill in Boso Peninsula, Japan. *Sedimentary Geology*, *80*(1–2), 67–75.
- Ito, M. & Masuda, F. (1989) Petrofacies of Paleo-Tokyo Bay sands, the Upper Pleistocene of central Honshu, Japan. In: Taira, A. & Masuda, F. (Eds.) *Sedimentary facies in the active plate margin*. Tokyo: Terra Scientific Publishing, pp. 179–196.
- Ito, M. & Saito, T. (2006) Gravel waves in an ancient canyon: analogous features and formative processes of coarse-grained bedforms in a submarine-fan system, the Lower Pleistocene of the Boso Peninsula, Japan. *Journal of Sedimentary Research*, *76*, 1274–1283.
- Jackson, C.A., McAndrew, A.E., Hodgson, D.M. & Dreyer, T. (2021) Repeated degradation and progradation of a submarine slope over geological timescales. *Journal of Sedimentary Research*, *91*, 116–145.
- Jobe, Z.R., Lowe, D.R. & Morris, W.R. (2012) Climbing-ripple successions in turbidite systems: depositional environments, sedimentation rates and accumulation times. *Sedimentology*, *59*, 867–898.
- Jones, A.P. & Omoto, K. (2000) Towards establishing criteria for identifying trigger mechanisms for soft-sediment deformation: a case study of Late Pleistocene lacustrine sands and clays, Onikobe and Nakayamadaira Basins, northeastern Japan. *Sedimentology*, *47*, 1211–1226.
- Joussain, R., Colin, C., Liu, Z., Meynadier, L., Fournier, L., Fauquembergue, K., Zaragosi, S., Schmidt, F., Rojas, V. & Bassinot, F. (2016) Climatic control of sediment transport from the Himalayas to the proximal NE Bengal Fan during the last glacial-interglacial cycle. *Quaternary Science Reviews*, *148*, 1–16.
- Kaizuka, S. (1987) Quaternary crustal movements in Kanto, Japan. *Chigaku Zasshi*, *96*, 223–240 (in Japanese with English abstract).
- Kajita, H., Maeda, A., Utsunomiya, M., Yoshimura, T., Ohkouchi, N., Suzuki, A. & Kawahata, H. (2021) Biomarkers in the rock outcrop of the Kazusa Group reveal palaeoenvironments of the Kuroshio region. *Communications Earth & Environment*, *2*, 82.
- Kamiya, N., Yamamoto, Y., Wang, Q., Kurimoto, Y., Zhang, F. & Takemura, T. (2017) Major variations in vitrinite reflectance and consolidation characteristics within a post-middle Miocene forearc basin, central Japan: a geodynamical implication for basin evolution. *Tectonophysics*, *710*, 69–80.
- Kamiya, N., Yamamoto, Y., Zhang, F. & Lin, W. (2020) Vitrinite reflectance and consolidation characteristics of the post-middle Miocene Forearc Basin in central and eastern Boso Peninsula, central Japan: implications for basin subsidence. *Island Arc*, *29*, e12344.
- Kane, I.A., Catterall, V., McCaffrey, W.D. & Martinsen, O.J. (2010) Submarine channel response to intrabasinal tectonics: the influence of lateral tilt. *AAPG Bulletin*, *94*, 189–219.
- Kane, I.A. & Pontén, A.S. (2012) Submarine transitional flow deposits in the Paleogene Gulf of Mexico. *Geology*, *40*, 1119–1122.
- Kane, I.A., Pontén, A.S., Vangdal, B., Eggenhuisen, J.T., Hodgson, D.M. & Spychala, Y.T. (2017) The stratigraphic record and processes of turbidity current transformation across deep-marine lobes. *Sedimentology*, *64*, 1236–1273.
- Kase, Y., Sato, M., Nishida, N., Ito, M., Mukti, M.M.R., Ikehara, K. & Takizawa, S. (2016) The use of microstructures for discriminating turbiditic and hemipelagic muds and mudstones. *Sedimentology*, *63*, 2066–2086.
- Katsura, Y. (1984) Depositional environments of the Plio-Pleistocene Kazusa Group, Boso Peninsula, Japan. *Association of Petroleum Geology*, *74*, 407–424.
- Kenyon, N.H. & Millington, J. (1995) Contrasting deepsea depositional systems in the Bering Sea. In: Pickering, K.T., Hiscott, R.N., Kenyon, N.H., Ricci Lucchi, F. & Smith, R.D.A. (Eds.) *Atlas of deep water environments: architectural style in turbidite systems*. London: Chapman and Hall, pp. 196–202. https://doi.org/10.1007/978-94-011-1234-5_28
- Kenyon, N.H., Millington, J., Droz, L. & Ivanov, M.K. (1995) Scour holes in a channel-lobe transition zone on the Rhône cone. In: Pickering, K.T., Hiscott, R.N., Kenyon, N.H., Ricci Lucchi, F. & Smith, R.D.A. (Eds.) *Atlas of deep water environments; architectural style in turbidite systems*. London: Chapman & Hall, pp. 212–215.
- Kikkawa, K., Mizuno, K. & Sugiyama, Y. (1991) Regional correlation of the early to middle Pleistocene Tephros in the Kanto and Kinki districts, Japan. *Earth Monthly*, *13*, 228–234 (in Japanese).
- Kioka, A., Schwestermann, T., Moernaut, J., Ikehara, K., Kanamatsu, T., Eglinton, T.I. & Strasser, M. (2019) Event stratigraphy in a hadal oceanic trench: the Japan trench as sedimentary archive recording recurrent giant subduction zone earthquakes and their role in organic carbon export to the deep sea. *Frontiers in Earth Science*, *7*, 319.
- Kitazato, H. (1989) Vertical distribution of benthic foraminifera within sediments (preliminary report). *Benthos Research (Bulletin Japanese Association Benthology)*, *35*, 41–51.
- Kneller, B.C. & McCaffrey, W.D. (2003) The interpretation of vertical sequences in turbidite beds: the influence of longitudinal flow structure. *Journal of Sedimentary Research*, *73*, 706–713.
- Kokelaar, B.P., Howells, M.F., Bevins, R.E., Roach, R.A. & Dunkley, P.N. (1984). The Ordovician marginal basin of Wales. In: Kokelaar, B.P. & Howells, M.F. (Eds.) *Marginal basin geology: volcanic and associated sedimentary and tectonic processes in modern and ancient marginal basins*. Geological Society, London, *Special Publications*, *16*, 245–269.
- Kuenen, PhH (1953) Graded bedding, with observations on Lower Paleozoic rocks of Britain: koninklijke Nederlandse Akademie van Wetenschappen. *Amsterdam, Afd. Natuurkunde Verhandelingen*, *22*, 47.
- Kuenen, PhH (1957) Sole markings of graded greywacke beds. *The Journal of Geology*, *65*, 231–258.
- Lanci, L., Tohver, E., Wilson, A. & Flint, S. (2013) Upper Permian magnetic stratigraphy of the lower Beaufort group, Karoo basin. *Earth and Planetary Science Letters*, *375*, 123–134.
- Liautaud, P.R., Hodell, D.A. & Huybers, P.J. (2020) Detection of significant climatic precession variability in early Pleistocene glacial cycles. *Earth and Planetary Science Letters*, *536*, 116137.
- Liu, G., Li, X., Chiang, H.W., Cheng, H., Yuan, S., Chawchai, S., He, S., Lu, Y., Aung, L.T., Maung, P.M., Tun, W.N., Oo, K.M. & Wang, X. (2020) On the glacial-interglacial variability of the

- Asian monsoon in speleothem $\delta^{18}\text{O}$ records. *Science Advances*, 6, 81–89.
- Lowe, D.R. (1975) Water escape structures in coarse-grained sediments. *Sedimentology*, 22, 157–204.
- Lowe, D.R. (1982) Sediment gravity flows; II, Depositional models with special reference to the deposits of high-density turbidity currents. *Journal of Sedimentary Research*, 52(1), 279–297.
- Lowe, D.R. & Guy, M. (2000) Slurry-flow deposits in the Britannia Formation (Lower Cretaceous), North Sea: a new perspective on the turbidity current and debris flow problem. *Sedimentology*, 47, 31–70.
- Lucchi, F.R. & Valmori, E. (1980) Basin-wide turbidites in a Miocene, over-supplied deep-sea plain: a geometrical analysis. *Sedimentology*, 27, 241–270.
- MacEachern, J.A., Bann, K.L., Bhattacharya, J.P. & Howell, C.D. Jr. (2005) Ichnology of deltas: organism responses to the dynamic interplay of rivers, waves, storms, and tides. In Giosan, L. & Bhattacharya, J.P. (Eds), *River deltas: concepts, models, and examples*. *SEPM, Special Publication*, 80, 49–85.
- Machida, H., Arai, F. & Sugihara, S. (1980) Tephrochronological study on the middle Pleistocene deposits in the Kanto and Kinki districts, Japan. *Quaternary Research*, 19, 233–261 (in Japanese).
- Maier, K.L., Paull, C.K., Caress, D.W., Anderson, K., Nieminski, N.M., Lundsten, E., Erwin, B.E., Gwiazda, R. & Fildani, A. (2020) Submarine-fan development revealed by integrated high-resolution datasets from La Jolla Fan, offshore California, USA. *Journal of Sedimentary Research*, 90, 468–479.
- Maier, K.L., Roland, E.C., Walton, M.A., Conrad, J.E., Brothers, D.S., Dartnell, P. & Kluesner, J.W. (2018) The tectonically controlled San Gabriel channel-lobe transition zone, Catalina Basin, southern California Borderland. *Journal of Sedimentary Research*, 88, 942–959.
- Mansor, H.E. & Amir Hassan, M.H. (2021) Facies and bed type characteristics of channel-lobe transition deposits from the Oligocene-Miocene Tajau Sandstone Member, Kudat Formation, Sabah, Malaysia. *Geological Journal*, 56, 5642–5672. <https://doi.org/10.1002/gj.426>
- McCave, I.N., Manighetti, B. & Robinson, S.G. (1995) Sortable silt and fine sediment size/composition slicing: parameters for palaeocurrent speed and palaeoceanography. *Paleoceanography*, 10, 593–610.
- McHargue, T., Pycz, M.J., Sullivan, M.D., Clark, J.D., Fildani, A., Romans, B.W., Covault, J.A., Levy, M., Posamentier, H.W. & Drinkwater, N.J. (2011) Architecture of turbidite channel systems on the continental slope: patterns and predictions. *Marine and Petroleum Geology*, 28, 728–743.
- McKay, M.P., Coble, M.A., Hessler, A.M., Weislogel, A.L. & Fildani, A. (2016) Petrogenesis and provenance of distal volcanic tuffs from the Permian-Triassic Karoo Basin, South Africa: a window into a dissected magmatic province. *Geosphere*, 12, 1–14.
- McKay, M.P., Weislogel, A.L., Fildani, A., Brunt, R.L., Hodgson, D.M. & Flint, S.S. (2015) U-PB zircon tuff geochronology from the Karoo Basin, South Africa: implications of zircon recycling on stratigraphic age controls. *International Geology Review*, 57, 393–410.
- Mitsunashi, T. (1954) Geology of the southern district of Kinadayama, Boso Peninsula- note on the extension of rock facies in time and space. *Geological Society of Japan*, 60, 461–472.
- Mitsunashi, T. (1961) Geological maps of the oil and gas field of Japan 4. Futtsu-Otaki, Geological Survey of Japan.
- Mitsunashi, T., Yasukuni, N. & Shinada, Y. (1959) Stratigraphical section of the Kazusa Group along the shores of the rivers Yoro and Obitsu. *Bulletin of the Geological Survey of Japan*, 10, 9–24 (in Japanese).
- Molenaar, A., Moernaut, J., Wiemer, G., Dubois, N. & Strasser, M. (2019) Earthquake impact on active margins: tracing surficial remobilization and seismic strengthening in a slope sedimentary sequence. *Geophysical Research Letters*, 46(11), 6015–6023.
- Momohara, A. (1994) Floral and paleoenvironmental history from the late Pliocene to middle Pleistocene in and around central Japan. *Palaeogeography, Palaeoclimatology, Palaeoecology*, 108, 281–293.
- Morris, E.A., Hodgson, D.M., Brunt, R.L. & Flint, S.S. (2014) Origin, evolution and anatomy of silt-prone submarine external levées. *Sedimentology*, 61, 1734–1763.
- Morris, S.A., Kenyon, N.H., Limonov, A.F. & Alexander, J. (1998) Downstream changes of large-scale bedforms in turbidites around the Valencia channel mouth, north-west Mediterranean: implications for palaeoflow reconstruction. *Sedimentology*, 45, 365–377. <https://doi.org/10.1046/j.1365-3091.1998.0160f.x>
- Mueller, P., Patacci, M. & Di Giulio, A. (2017) Hybrid event beds in the proximal to distal extensive lobe domain of the coarse-grained and sand-rich Bordighera turbidite system (NW Italy). *Marine and Petroleum Geology*, 86, 908–931.
- Mutti, E. (1985) Turbidite systems and their relations to depositional sequences. In: *Provenance of arenites*. Dordrecht: Springer, pp. 65–93.
- Mutti, E. (1992) Turbidite sandstones. Agip: Istituto di geologia, Università di Parma.
- Mutti, E. & Nilsen, T.H. (1981). Significance of intraformational rip-up clasts in deep-sea fan deposits. International Association of Sedimentologists. 2nd European Regional Meeting. Abstract, Bologna, pp. 117–119.
- Mutti, E., Nilsen, T.H. & Ricci Lucchi, F. (1978) Outer fan depositional lobes of the Laga Formation (Upper Miocene and Lower Pliocene), east-central Italy. In: Stanley, D.J. & Kelling, G. (Eds.) *Sedimentation in submarine canyons, fans, and trenches*. Stroudsburg: Dowden, Hutchinson and Ross, pp. 210–223.
- Mutti, E. & Normark, W.R. (1987) Comparing examples of modern and ancient turbidite systems: problems and concepts. In: Legget, J.K. & Zuffa, G.G. (Eds.) *Marine clastic sedimentology: concepts and case studies*. London: Graham and Trotman, pp. 1–38.
- Mutti, E. & Normark, W.R. (1991) An integrated approach to the study of turbidite systems. In: Weimer, P. & Link, M.H. (Eds.) *Seismic facies and sedimentary processes of submarine fans and turbidite systems*. New York, NY: Springer, pp. 75–106.
- Mutti, E. & Sonnino, M. (1981) Compensation cycles: a diagnostic feature of turbidite sandstone lobes. In International Association of Sedimentologists-European Regional Meeting 2, 120–123.
- Muzzi Magalhaes, P. & Tinterri, R. (2010) Stratigraphy and depositional setting of slurry and contained (reflected) beds in the Marnoso-arenacea Formation (Langhian-Serravallian) Northern Apennines, Italy. *Sedimentology*, 57(7), 1685–1720.
- Nakajima, J., Katayama, H. & Itaki, T. (2009). Climatic control on turbidite deposition during the last 70 kyr along the Toyama deep-sea channel, central Japan Sea. In: Kneller, B., Martinsen,

- O.J. & McCaffrey, B. (Eds.) *External controls on deep-water depositional systems*. SEPM Special Publication No. 92 SEPM (Society for Sedimentary Geology), Tulsa, pp. 159–177.
- Naruse, Y. (1968). Quaternary crustal movements in the Kanto region. In Nakagawa, H. (Ed.), *Quaternary crustal movements. Memoirs of the Geological Society of Japan*, 2, 29–32 (in Japanese).
- Nishida, N., Ajioka, T., Ikehara, K., Nakashima, R., Katayama, H., Sato, T., Furuyama, S. & Tamura, T. (2020) Postglacial stratigraphic evolution of a current-influenced sandy shelf: off-shore Kujukuri strandplain, central Japan. *Sedimentology*, 67, 559–575.
- Nishida, N. & Ikehara, K. (2013) Holocene evolution of depositional processes off southwest Japan: response to the Tsushima Warm Current and sea-level rise. *Sedimentary Geology*, 290, 138–148.
- Normark, W.R., Piper, D.J.W. & Hess, G.R. (1979) Distributary channels, sand lobes, and mesotopography of Navy submarine fan, California Borderland, with applications to ancient fan sediments. *Sedimentology*, 26, 749–774. <https://doi.org/10.1111/j.1365-3091.1979.tb00971.x>
- Palanques, A., Kenyon, N.H., Alonso, B. & Limonov, A.F. (1995) Erosional and depositional patterns in the Valencia channel mouth: an example of a modern channel-lobe transition zone. *Marine Geophysical Researches*, 18, 103–118. <https://doi.org/10.1007/BF01204341>
- Peakall, J., Best, J.L., Baas, J., Hodgson, D.M., Clare, M.A., Talling, P.J., Dorrell, R.M. & Lee, D.R. (2020) An integrated process-based model of flutes and tool marks in deep-water environments: implications for palaeohydraulics, the Bouma sequence, and hybrid event beds. *Sedimentology*, 67, 1601–1666.
- Pemberton, E.A., Hubbard, S.M., Fildani, A., Romans, B. & Stright, L. (2016) The stratigraphic expression of decreasing confinement along a deep-water sediment routing system: outcrop example from southern Chile. *Geosphere*, 12, 114–134.
- Pickering, K.T., Souter, C., Oba, T., Taira, A., Schaaf, M. & Platzman, E. (1999) Glacio-eustatic control on deep-marine clastic forearc sedimentation, Pliocene-mid-Pleistocene (c. 1180–600 ka) Kazusa Group, SE Japan. *Journal of the Geological Society*, 156, 125–136.
- Pierce, C.S., Haughton, P.D., Shannon, P.M., Pulham, A.J., Barker, S.P. & Martinsen, O.J. (2018) Variable character and diverse origin of hybrid event beds in a sandy submarine fan system, Pennsylvanian Ross Sandstone Formation, western Ireland. *Sedimentology*, 65, 952–992.
- Posamentier, H.W. (2003) Depositional elements associated with a basin floor channel-levee system: case study from the Gulf of Mexico. *Marine and Petroleum Geology*, 20, 677–690.
- Postma, G., Hilgen, F.J. & Zachariasse, W.J. (1993) Precession-punctuated growth of a late Miocene submarine-fan lobe on Gavdos (Greece). *Terra Nova*, 5, 438–444.
- Prather, B.E. (2000) Calibration and visualization of depositional process models for above-grade slopes: a case study from the Gulf of Mexico. *Marine and Petroleum Geology*, 17, 619–638.
- Prather, B.E. (2003) Controls on reservoir distribution, architecture and stratigraphic trapping in slope settings. *Marine and Petroleum Geology*, 20, 529–545. <https://doi.org/10.1016/j.marpetgeo.2003.03.009>
- Prather, B.E., O'Byrne, C., Pirmez, C. & Sylvester, Z. (2017) Sediment partitioning, continental slopes and base-of-slope systems. *Basin Research*, 29, 394–416.
- Prélat, A., Covault, J.A., Hodgson, D.M., Fildani, A. & Flint, S.S. (2010) Intrinsic controls on the range of volumes, morphologies, and dimensions of submarine lobes. *Sedimentary Geology*, 232, 66–76.
- Prélat, A., Hodgson, D.M. & Flint, S.S. (2009) Evolution, architecture and hierarchy of distributary deep-water deposits: a high-resolution outcrop investigation from the Permian Karoo Basin, South Africa. *Sedimentology*, 56, 2132–2154.
- Prins, M.A., Postma, G. & Weltje, G.J. (2000) Controls on terrigenous sediment supply to the Arabian Sea during the late Quaternary: the Makran continental slope. *Marine Geology*, 169, 351–371.
- Privat, A.M.L., Hodgson, D.M., Jackson, C.A.L., Schwarz, E. & Peakall, J. (2021) Evolution from syn-rift carbonates to early post-rift deep-marine intraslope lobes: the role of rift basin physiography on sedimentation patterns. *Sedimentology*, 68, 2563–2605. <https://doi.org/10.1111/SED.12864>
- Pyles, D.R., Strachan, L.J. & Jennette, D.C. (2014) Lateral juxtapositions of channel and lobe elements in distributive submarine fans: three-dimensional outcrop study of the Ross Sandstone and geometric model. *Geosphere*, 10, 1104–1122.
- Pyrzcz, M.J., Catuneanu, O. & Deutsch, C.V. (2005) Stochastic surface-based modeling of turbidite lobes. *AAPG Bulletin*, 89, 177–191.
- Rice, J.A., Simms, A.R., Buzas-Stephens, P., Steel, E., Livsey, D., Reynolds, L.C., Yokoyama, Y. & Halihan, T. (2020) Deltaic response to climate change: the Holocene history of the Nueces Delta. *Global and Planetary Change*, 191, 103213.
- Sato, T. & Koike, K. (1957) A fossil submarine canyon near the southern foot of Mt. Kano, Tiba Prefecture. *Journal of the Geological Society of Japan*, 63, 100–116 (in Japanese).
- Satoguchi, Y. (1995) Tephrostratigraphy in the lower to middle Kazusa Group in the Boso Peninsula. *Geological Society of Japan*, 101, 767–782 (Japanese).
- Satoguchi, Y. & Nagahashi, Y. (2012) Tephrostratigraphy of the Pliocene to Middle Pleistocene series in Honshu and Kyushu islands, Japan. *Island Arc*, 21, 49–169.
- Schwestermann, T., Huang, J., Konzett, J., Kioka, A., Wefer, G., Ikehara, K., Moernaut, J., Elginton, T.I. & Strasser, M. (2020) Multivariate statistical and multiproxy constraints on earthquake-triggered sediment remobilization processes in the central Japan Trench. *Geochemistry, Geophysics, Geosystems*, 21, e2019GC008861.
- Seno, T., Sakurai, T. & Stein, S. (1996) Can the Okhotsk plate be discriminated from the North American plate? *Journal of Geophysical Research*. *Solid Earth*, 101, 11305–11315.
- Sequeiros, O.E., Mosquera, R. & Pedocchi, F. (2018) Internal structure of a self-accelerating turbidity current. *Journal of Geophysical Research: Oceans*, 123, 6260–6276.
- Sequeiros, O.E., Naruse, H., Endo, N., Garcia, M.H. & Parker, G. (2009) Experimental study on self-accelerating turbidity currents. *Journal of Geophysical Research: Oceans*, 114, C05025.
- Shishikura, M., Haraguchi, T. & Miyauchi, T. (2001) Timing and recurrence interval of the Taisho-type Kanto Earthquake, analyzing Holocene emerged shoreline topography in the Iwai Lowland, the southwestern part of the Boso Peninsula, central Japan. *Jishin*, 53, 357–372.
- Sixsmith, P.J., Flint, S.S., Wickens, H.D. & Johnson, S.D. (2004) Anatomy and stratigraphic development of a basin floor turbidite system in the Laingsburg Formation, Main Karoo Basin, South Africa. *Journal of Sedimentary Research*, 74, 239–254.

- Smith, R.M.H., Eriksson, P.G. & Botha, W.J. (1993) A review of the stratigraphy and sedimentary environments of the Karoo-aged basins of Southern Africa. *Journal of African Earth Sciences (and the Middle East)*, *16*, 143–169.
- Sohn, Y.K. (1997) On traction-carpet sedimentation. *Journal of Sedimentary Research*, *67*, 502–509.
- Southern, S.J., Patacci, M., Felletti, F. & McCaffrey, W.D. (2015) Influence of flow containment and substrate entrainment upon sandy hybrid event beds containing a co-genetic mud-clast-rich division. *Sedimentary Geology*, *321*, 105–122.
- Spychala, Y.T., Hodgson, D.M. & Lee, D.R. (2017b) Autogenic controls on hybrid bed distribution in submarine lobe complexes. *Marine and Petroleum Geology*, *88*, 1078–1093.
- Spychala, Y.T., Hodgson, D.M., Prélat, A., Kane, I.A., Flint, S.S. & Mountney, N.P. (2017a) Frontal and lateral submarine lobe fringes: comparing sedimentary facies, architecture and flow processes. *Journal of Sedimentary Research*, *87*, 75–96.
- Spychala, Y.T., Ramaaker, T.A., Eggenhuisen, J.T., Grundvåg, S.A., Pohl, F. & Wroblewska, S. (2021) Proximal to distal grain-size distribution of basin-floor lobes: a study from the Battfjellet Formation, Central Tertiary Basin, Svalbard. *The Depositional Record*. 167.
- Stevenson, C.J., Jackson, C.A.L., Hodgson, D.M., Hubbard, S.M. & Eggenhuisen, J.T. (2015) Deep-water sediment bypass. *Journal of Sedimentary Research*, *85*, 1058–1081.
- Stevenson, C.J., Peakall, J., Hodgson, D.M., Bell, D. & Privat, A. (2020) T_b or not T_b : banding in turbidite sandstones. *Journal of Sedimentary Research*, *90*, 821–842.
- Stevenson, C.J., Talling, P.J., Masson, D.G., Sumner, E.J., Frenz, M. & Wynn, R.B. (2014a) The spatial and temporal distribution of grain-size breaks in turbidites. *Sedimentology*, *61*, 1120–1156.
- Stevenson, C.J., Talling, P.J., Sumner, E.J., Masson, D.G., Frenz, M. & Wynn, R.B. (2014b) On how thin submarine flows transported large volumes of sand for hundreds of kilometres across a flat basin plain without eroding the sea floor. *Sedimentology*, *61*, 1982–2019.
- Stevenson, C.J., Talling, P.J., Wynn, R.B., Masson, D.G., Hunt, J.E., Frenz, M., Akhmetzhanov, A. & Cronin, B.T. (2013) The flows that left no trace: very large-volume turbidity currents that bypassed sediment through submarine channels without eroding the sea floor. *Marine and Petroleum Geology*, *41*, 186–205.
- Suganuma, Y., Okada, M., Head, M.J., Kameo, K., Haneda, Y., Hayashi, H., Irizuki, T., Itaki, T., Izumi, K., Kubota, Y., Nakazato, H., Nishida, N., Okuda, M., Satoguchi, Y., Simon, Q. & Takeshita, Y. (2021) Formal ratification of the global boundary stratotype section and point (GSSP) for the Chibanian stage and middle Pleistocene subseries of the Quaternary system: the Chiba section, Japan. *Episodes*, *44*, 317–347. <https://doi.org/10.18814/epiiugs/2020/020080>
- Sugiyama, N. & Miyata, Y. (2015) Sediment supply and transport pass inferred from magnetic susceptibility of submarine fan deposits of the Kazusa Group. 10th Asian Regional Conference of IAEG.
- Sumner, E.J., Talling, P.J. & Amy, L.A. (2009) Deposits of flows transitional between turbidity current and debris flow. *Geology*, *37*, 991–994.
- Suzuki, M. & Sugihara, S. (1983) Fission-track age constraints on the Plio-Pleistocene boundary in the Kazusa Group. Abstract, Annual Meeting of the Japanese Association of Quaternary Research, 13, 69–70 (in Japanese).
- Sweet, M.L. & Blum, M.D. (2016) Connections between fluvial to shallow marine environments and submarine canyons: implications for sediment transfer to deep water. *Journal of Sedimentary Research*, *86*, 1147–1162.
- Sylvester, Z. & Lowe, D.R. (2004) Textural trends in turbidites and slurry beds from the Oligocene flysch of the East Carpathians, Romania. *Sedimentology*, *51*, 945–972.
- Takano, S., Ito, M., Nakano, T., Horikawa, K., Nakamura, Y. & Saito, T. (2004) Sequence-stratigraphic signatures of hemipelagic siltstones in deep-water successions: the Lower Pleistocene Kiwada and Otadai Formations, Boso Peninsula, Japan. *Sedimentary Geology*, *170*, 189–206.
- Takao, A., Nakamura, K., Takaoka, S., Fuse, M., Oda, Y., Shimano, Y., Nishida, N. & Ito, M. (2020) Spatial and temporal variations in depositional systems in the Kazusa Group: insights into the origins of deep-water massive sandstones in a Pleistocene forearc basin on the Boso Peninsula, Japan. *Progress in Earth and Planetary Science*, *7*, 37.
- Talling, P.J., Amy, L.A., Wynn, R.B., Peakall, J. & Robinson, M. (2004) Beds comprising debrite sandwiched within co-genetic turbidite: origin and widespread occurrence in distal depositional environments. *Sedimentology*, *51*, 163–194.
- Talling, P.J., Masson, D.G., Sumner, E.J. & Malgesini, G. (2012) Subaqueous sediment density flows: depositional processes and deposit types. *Sedimentology*, *59*, 1937–2003.
- Terlaky, V. & Arnott, R.W.C. (2014) Matrix-rich and associated matrix-poor sandstones: avulsion splays in slope and basin-floor strata. *Sedimentology*, *61*, 1175–1197.
- Tinterri, R., Muzzi Magalhaes, P., Tagliaferri, A. & Cunha, R.S. (2016) Convolute laminations and load structures in turbidites as indicators of flow reflections and decelerations against bounding slopes. Examples from the Marnoso-arenacea Formation (northern Italy) and Annot Sandstones (south eastern France). *Sedimentary Geology*, *344*, 382–407.
- Tsuji, T., Miyata, Y., Okada, M., Mita, I., Nakagawa, H., Sato, Y. & Nakamizu, M. (2005) High-resolution chronology of the lower Pleistocene Otadai and Umegase Formations of the Kazusa Group, Boso Peninsula, central Japan (Chronostratigraphy of the JNOC TR-3 cores based on oxygen isotope, magnetostratigraphy and calcareous nannofossil). *Journal of the Geological Society of Japan*, *111*, 1–20 (in Japanese with English abstract).
- Van der Merwe, W.C., Hodgson, D.M., Brunt, R.L. & Flint, S.S. (2014) Depositional architecture of sand-attached and sand-detached channel-lobe transition zones on an exhumed stepped slope mapped over a 2500 km² area. *Geosphere*, *10*, 1076–1093.
- Walker, R.G. (1992) Facies, facies models and modern stratigraphic concepts. In: Walker, R.G. & James, N.P. (Eds.) *Facies models: response to sea-level change*. St John's: Geological Association of Canada, pp. 1–14.
- Weltje, G. & de Boer, P.L. (1993) Astronomically induced paleoclimatic oscillations reflected in Pliocene turbidite deposits on Corfu (Greece): implications for the interpretation of higher order cyclicity in ancient turbidite systems. *Geology*, *21*, 307–310.
- Winterwerp, J.C. & van Kesteren, W.G.M. (2004) *Introduction to the physics of cohesive sediments in the marine environment, developments in sedimentology*, vol. 56. New York: Elsevier, 466 pp.
- Wynn, R.B., Kenyon, N.H., Masson, D.G., Stow, D.A. & Weaver, P.P. (2002) Characterization and recognition of deep-water channel-lobe transition zones. *AAPG Bulletin*, *86*, 1441–1462.
- Wynn, R.B. & Stow, D.A. (2002) Classification and characterisation of deep-water sediment waves. *Marine Geology*, *192*(1–3), 7–22.

- Yamauchi, S., Mitsunashi, T. & Okubo, S. (1990) Growth pattern of the early Pleistocene Higashihigasa submarine channel, Boso Peninsula, Japan. *Geological Society of Japan, Journal*, 96, 523–536.
- Zhang, Y., Zhang, Z., Chen, D., Qiu, B. & Wang, W. (2020) Strengthening of the Kuroshio current by intensifying tropical cyclones. *Science*, 368(6494), 988–993.

SUPPORTING INFORMATION

Additional supporting information may be found in the online version of the article at the publisher's website.

How to cite this article: Brooks, H.L., Ito, M., Zuchuat, V., Peakall, J. & Hodgson, D.M. (2022) Channel-lobe transition zone development in tectonically active settings: Implications for hybrid bed development. *The Depositional Record*, 8, 829–868. Available from: <https://doi.org/10.1002/dep2.180>